European Journal of Medicinal Chemistry 217 (2021) 113363

Contents lists available at ScienceDirect

European Journal of Medicinal Chemistry

journal homepage: http://www.elsevier.com/locate/ejmech

Novel dual-mode antitumor chlorin-based derivatives as potent photosensitizers and histone deacetylase inhibitors for photodynamic therapy and chemotherapy

Xing-Jie Zhang [a, 1], Ming-Hui Liu [b, 1], Yu-Sha Luo [a, 1], Gui-Yan Han [a], Zhi-Qiang Ma [a], Fei Huang [a], Yuan Wang [c], Zhen-Yuan Miao [a], Wan-Nian Zhang [a], Chun-Quan Sheng [a], Jian-Zhong Yao [a, b, c, *]

[a] School of Pharmacy, Second Military Medical University, Shanghai, 200433, China
[b] Department of Pharmacy, Fujian University of Traditional Chinese Medicine, Fuzhou, 350108, China
[c] School of Pharmacy, Ningxia Medical University, Yinchuan, 750004, China

ARTICLE INFO

Article history:
Received 20 December 2020
Received in revised form
14 February 2021
Accepted 27 February 2021
Available online 17 March 2021

Keywords:
Photodynamic therapy
Photosensitizer
Histone deacetylase inhibitor (HDACI)
Talaporfin

ABSTRACT

The combination of photodynamic therapy (PDT) and chemotherapy is a prospective strategy to improve antitumor efficacy. Herein, a series of novel cytotoxic chlorin-based derivatives as dual photosensitizers (PSs) and histone deacetylase inhibitors (HDACIs) were synthesized and investigated for biological activity. Among them, compound **15e** showed definite HDAC2 and 10 inhibitory activities by up-regulating expression of acetyl-H4 and highest phototoxicity and dark-toxicity, which was more phototoxic than Talaporfin as a PS while with stronger dark-toxicity compared to vorinostat (SAHA) as a HDACI. The biological assays demonstrated that **15e** was liable to enter A549 cells and localized in mitochondria, lysosomes, golgi and endoplasmic reticulum (ER) etc. multiple organelles, resulting in higher cell apoptosis rate and ROS production compared to Talaporfin. Moreover, it could induce tumor cell autophagy as a dual PS and HDACI. All results suggested that compound **15e** could be applied as a potential dual cytotoxic drug for PDT and chemotherapy.

© 2021 Elsevier Masson SAS. All rights reserved.

1. Introduction

Photodynamic therapy (PDT) has been a unique noninvasive therapeutic modality for a range of cancers through generating cytotoxic reactive oxygen species (ROS) induced by photosensitizers (PSs) combined with light irradiation, resulting in cell death and tumor ablation. The characteristics of PSs have a tremendous effect on PDT efficacy, and PSs of various structures have been approved for clinical use or under investigation in clinical trials, such as photofrin (Porfimer Sodium), 5-ALA, Verteporfin (BPD-MA), Talaporfin (Npe6), Temoporfin (m-THPC, Foscan), Padeliporfin (Tookad Soluble, WST-11), HPPH, etc [1–4]. As a type of structurally nonspecific drugs, however, PSs suffer from some defects such as lack of specific drug-target and selectivity for tumor tissue, less effective activity for huge solid tumors and metastatic tumors, etc [5,6]. Focused on the shortcomings, further improvements in PDT necessitate that PSs target more selectively tumor tissues [7,8]. Relevant research has recently shown that PSs conjugated to biomacromolecules with targeting function such as peptide [9], protein [10], transferrin and aptamer [11,12], or small molecules such as folic acid [13–15], amino acid [16–19] and saccharide [20,21], will increase the tumor selectivity. Furthermore, PDT combining other therapeutic methods such as chemotherapy [22–24], photothermal therapy [25,26], immunotherapy [27], etc. will obtain additive or synergistic effects as well.

Targeting proteins relevant to epigenetic regulation has emerged as an appealing therapeutic protocol for the treatment of cancer [28]. Among the numerous epigenetic enzymes, histone deacetylase (HDAC), which can catalyze the deacetylation from lysine residues thus bringing about controlling the transcriptional regulation, cell proliferation and apoptosis, has become one of the hot targets for cancer treatment [29–31]. Hitherto, several HDAC inhibitors (HDACIs) including vorinostat (SAHA), romidepsin

* Corresponding author. School of Pharmacy, Second Military Medical University, Shanghai, 200433, China.
E-mail address: yaojz6601@sina.com (J.-Z. Yao).
[1] These authors contributed equally to this work.

https://doi.org/10.1016/j.ejmech.2021.113363
0223-5234/© 2021 Elsevier Masson SAS. All rights reserved.

(FK228), belinostat (PXD101), panobinostat (LBH589) and chidamide (CS005), have been approved for the clinical treatment of hematologic cancer [32–35]. Generally, most HDACIs include three structural parts: a hydrophobic cap group, a linker (alkyl, alkenyl, or aryl), and a zinc binding group (ZBG, hydroxamic acid or benzamide) (Fig. 1A) [36]. As active non-essential group, the cap group interacts with the surface of HDAC and can be replaced by other structure to design diverse multi-target drugs [37]. Despite the demonstrated efficacy in hematological tumors, HDACIs has disappointingly not exhibited such success in solid tumors maybe due to their poor pharmacokinetics [38], thereby ultimately resulting in inadequate ability to reach therapeutic concentrations [39,40]. It is notable that there have been successful examples of HDACIs in the treatment of solid tumors when using original prodrug or multi-target-drug design [41,42].

Related research has found that the HDAC activity in residual cancerous cells would be improved after PDT, leading to the potential recrudesce and metastasis of tumor [43]. It has been also reported that the HDACIs possessed synergistic anticancer effects when combining with PSs [44,45]. It is thus clear that the combination of PDT and chemotherapy is a prospective strategy to improve anticancer efficiency. It is, therefore, expected that PSs conjugated to pharmacophore of HDACI via linker group would exhibit dual cytotoxic efficacy for PDT and chemotherapy.

Our research group previously had synthesized a great number of chlorin-type classical candidate PSs with high PDT cytotoxic efficiency and low toxicity such as benzochloroporphyrin derivatives (BCPDs) [46–48], amino acid derivatives of pyropheophorbide-a ethers [16] and chlorin p_6-based amino acid derivatives [17,18]. To further improve antitumor efficacy and overcome potential recurrence and metastasis of tumor induced by the increase of HDAC activity after PDT treatment, we rationally designed a series of novel chlorin-based derivatives with dual cytotoxic activity of PDT and chemotherapy. The designed target compounds were synthesized by coupling the ZBG on 17^3-propionyloxy of chlorophyll-a stable degradation products chlorin p_6-13^1,15^1-dimethylester (**7**) and chlorin f-13^1-monomethylester (**8**) (Fig. 1B and Scheme 1) via linker including aliphatic and aromatic carbon chains (Fig. 1C, Scheme 2, Scheme 3 and Scheme 4), and systematically evaluated their photophysical properties, cytotoxic efficacy and biological mechanism.

2. Results and discussion

2.1. Synthesis

As shown in Scheme 1, chlorin f (**5**) and chlorin p_6-13^1,15^1-dimethylester (**7**) were prepared according to our previously established protocol using crude chlorophyll extracts from Chinese traditional herb named silkworm excrement as the starting material [16,49]. **5** was then reacted with freshly prepared diazomethane to give chlorin f-13^1,17^3-dimethylester, which was selectively hydrolyzed in THF with 25% aqueous HCl to afford chlorin f-13^1-monomethylester (**8**).

The synthesis of *o*-phenylenediamine and hydroxamic acid derivatives of compound **7** linked by aliphatic carbon chain is outlined in Scheme 2. **7** was coupled with *o*-phenylenediamine in presence of O-benzotriazol-1-yl-*N*,*N*,*N*′*N*′-tetramethyluronium hexafluorophosphate (HBTU) and *N*,*N*-diisopropylethylamine (DIPEA) to obtain the *o*-phenylenediamine-type target compound **10a** in yield of 62.2%. The 17^3-carboxylic acid of **7** was activated using *N*-hydroxysuccinimide (NHS) in presence of 1-(3-dimethylaminopropyl)-3-ethylcarbodiimide hydrochloride (EDCI) and 4-dimethylaminopyridine (DMAP), and then individually reacted with 4-aminobutyric acid, 5-aminovaleric acid or 6-aminocaproic acid to form three intermediates **9b**, **9c** and **9d**, which were coupled with *o*-phenylenediamine in presence of HBTU and DIPEA to produce the *o*-phenylenediamine-type target

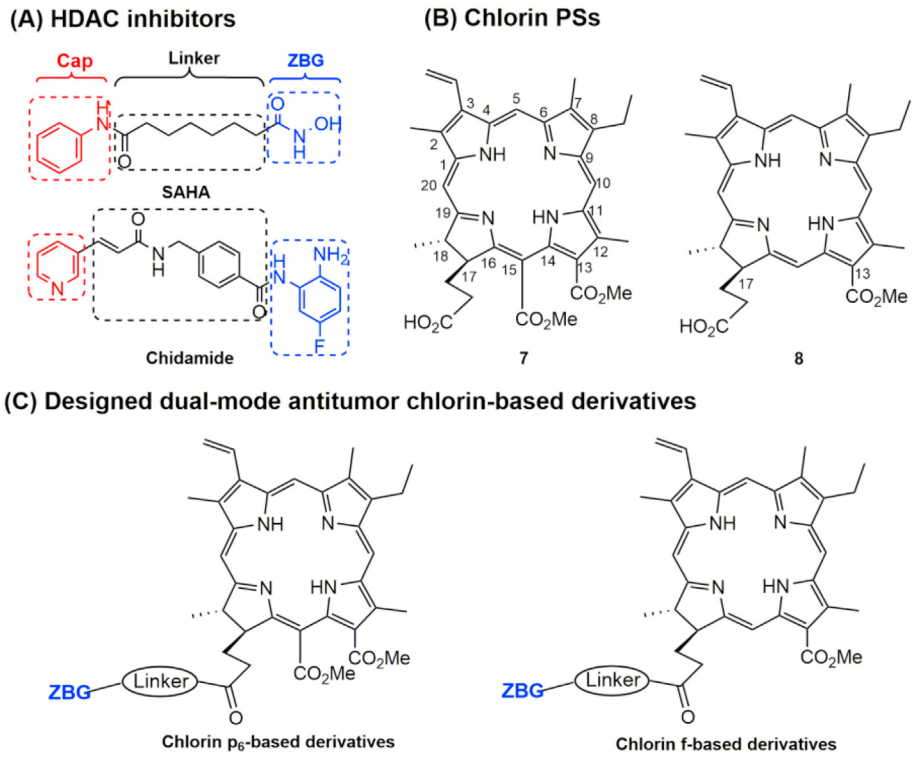

Fig. 1. Chemical features of HDACIs (**A**) lead chlorin PSs (**B**) and target dual-mode cytotoxic chlorin-based derivatives.

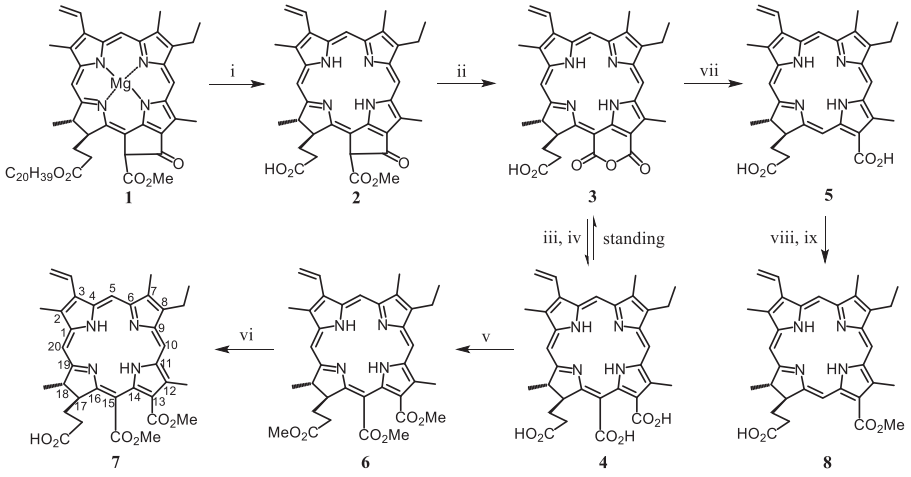

Scheme 1. Reagents and conditions: (i) 36% HCl, Et_2O, 0–5 °C, 0.5 h; (ii) KOH, *i*-PrOH-Et_2O, O_2, r.t., 12 h, 34.4%; (iii) THF-MeOH-aqueous NaOH (0.5 mol/L) (1:4:5, *v/v/v*), r.t., 1 h; (iv) 0.5 mol/L aqueous HCl to adjust pH value to 5–6, extraction with Et_2O; (v) CH_2N_2–Et_2O, r.t., 0.5 h, 83.6% (from c to e); (vi) THF-25% aqueous HCl (1:1, *v/v*), r.t., 4 h, 81.8%; (vii) 25% KOH–EtOH, N_2, reflux, 1 h; (viii) CH_2N_2–Et_2O, 0 °C, 10 min; (ix) THF-25% aqueous HCl (1:1, *v/v*), r.t., 4 h.

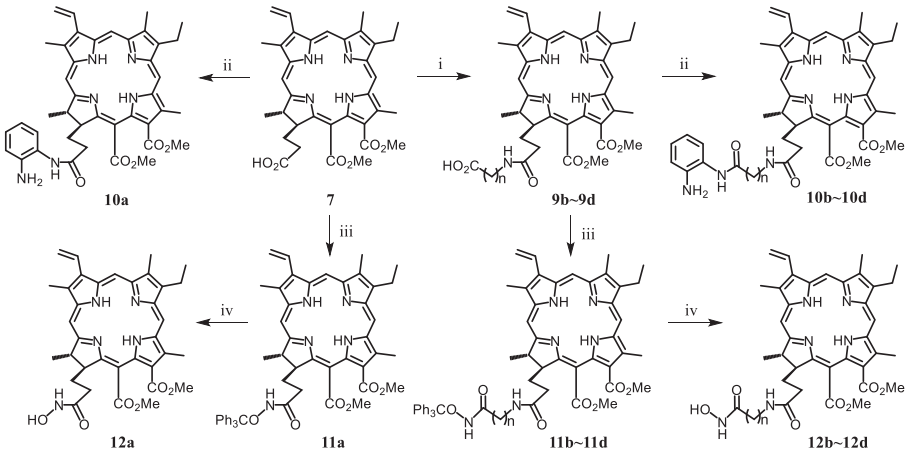

Scheme 2. Reagents and conditions: (i) NHS, EDCI, DMAP, r.t., 24 h; 4-aminobutyric acid (**b**: n = 3) or 5-aminovaleric acid (**c**: n = 4) or 6-aminocaproic acid (**d:** n = 5), r.t., 48 h; (ii) *o*-phenylenediamine, HBTU, DIPEA, r.t., 12 h; (iii) HATU, DIPEA, r.t., 0.5 h; O-tritylhydroxylamine, r.t., 24 h; (iv) $BF_3 \cdot Et_2O$, 0 °C, 2 h.

compounds **10b**, **10c**, and **10c** in yields of 45.6%, 43.2% and 48.5%, respectively. In addition, compound **7**, **9a**, **9b** and **9c** were reacted with O-tritylhydroxylamine in presence of 2-(7-azabenzotriazol-1-yl)-*N*,*N*,*N*′,*N*′-tetramethyluronium hexafluorophosphate (HATU) and DIPEA to form the intermediates **11a**, **11b**, **11c** and **11d**, which were followed by cleavage of their triphenylmethyl with $BF_3 \cdot Et_2O$ to obtain the hydroxamic acid-type target compounds **12a**, **12b**, **12c** and **12d** in yields of 43.6%, 32.1%, 29.2% and 33.6%, respectively.

The synthesis of *o*-phenylenediamine and hydroxamic acid derivatives of compound **7** linked by aromatic carbon chain is illustrated in Scheme 3. **7** was individually reacted with 4-aminobenzoic acid *tert*-butyl ester (**e**), 3-aminocinnamic acid *tert*-butyl ester (**f**) or 4-aminocinnamic acid *tert*-butyl ester (**g**) in presence of HATU and DIPEA to afford compounds **13e**, **13f** and **13g**, following by removal of their *tert*-butyl with trifluoroacetic acid (TFA) to form key intermediates **14e**, **14f** and **14g**, which were coupled with *o*-phenylenediamine in presence of HBTU and DIPEA to obtain the *o*-phenylenediamine-type target compounds **15e**, **15f**, and **15g** in yields of 41.2%, 39.4% and 40.9%, respectively. Meanwhile, intermediates **14e**, **14f** and **14g** were reacted with O-tritylhydroxylamine in presence of DIPEA and HATU to give compounds **16e**, **16f** and **16g**, which were followed by cleavage of their triphenylmethyl with $BF_3 \cdot Et_2O$ to obtain the hydroxamic acid type target compounds **17e**, **17f** and **17g** in yields of 31.1%, 29.0% and 30.6%, respectively.

The synthesis of hydroxamic acid derivatives of compound **8** linked by aromatic carbon chain is graphically presented in Scheme 4. As a similar to the procedure for the synthesis of **17e** and **17g**, **8** was individually reacted with 4-aminobenzoic acid *tert*-butyl ester (**e**) or 4-aminocinnamic acid *tert*-butyl ester (**g**) to get crude products **18e** and **18g** whose *tert*-butyl protective group of carboxyl was removed by TFA to give **19e** and **19g**, which were coupled with O-tritylhydroxylamine, following by removal of O-triphenylmethyl protective group with $BF_3 \cdot Et_2O$ to obtain hydroxamic acid type target compounds **20e** and **20g** in yields of 41.0% and 40.4%, respectively.

2.2. Photophysical properties

Photophysical properties of a PS are significant parameters to determine PDT conditions and evaluate its efficacy. As shown in Fig. 2, maximum absorption wavelength in visible bands of chlorin

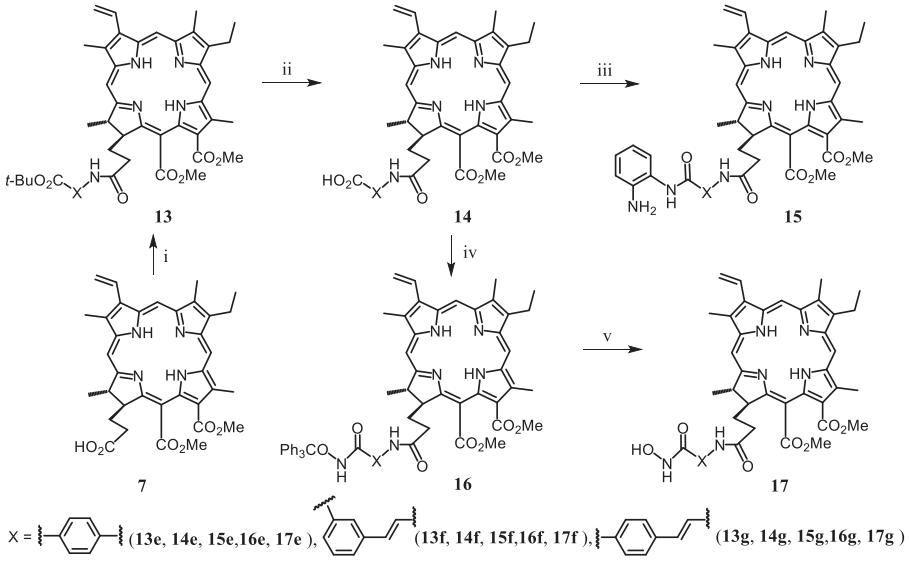

Scheme 3. Reagents and conditions: (i) 4-aminobenzoic acid *tert*-butyl ester (**e**) or 3-aminocinnamic acid *tert*-butyl ester (**f**) or 4-aminocinnamic acid *tert*-butyl ester (**g**), HATU, DIPEA, r.t., 48 h; (ii) TFA, 0 °C, 4 h; (iii) *o*-phenylenediamine, HBTU, DIPEA, r.t., 12 h; (iv) HATU, DIPEA, r.t., 0.5 h; O-tritylhydroxylamine, r.t., 24 h; (v) $BF_3{\cdot}Et_2O$, 0 °C, 2 h.

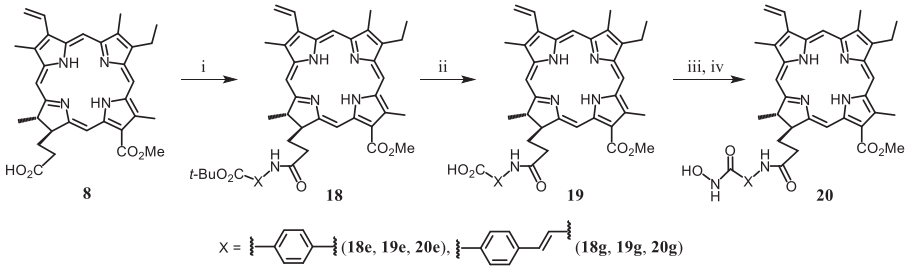

Scheme 4. Reagents and conditions: (i) 4-aminobenzoic acid *tert*-butyl ester (**e**) or 4-aminocinnamic acid *tert*-butyl ester (**g**), HATU, DIPEA, r.t., 48 h; (ii) TFA, 0 °C, 4 h; (iii) HATU, DIPEA, r.t., 0.5 h; O-tritylhydroxylamine, r.t., 24 h; (iv) $BF_3{\cdot}Et_2O$, 0 °C, 2 h.

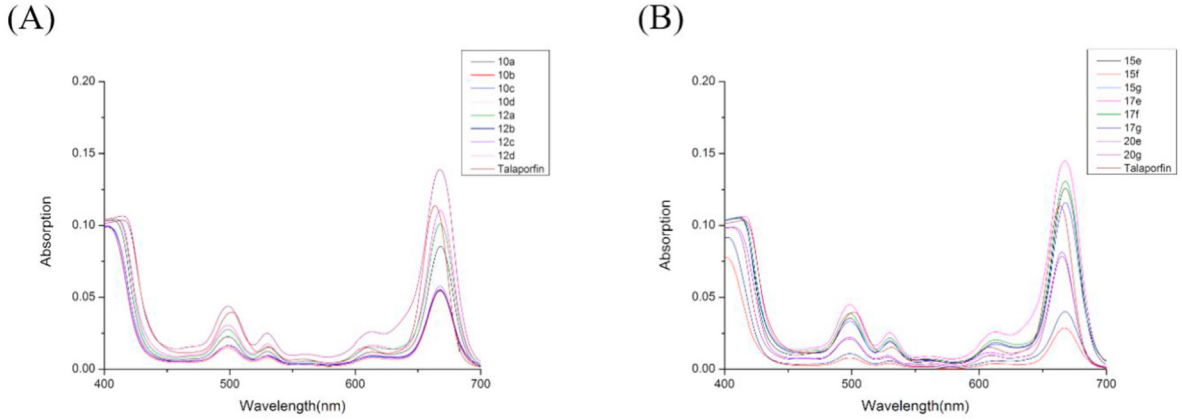

Fig. 2. UV absorption spectra of hydroxamic acid and *o*-phenylenediamine derivatives of chlorin linked with aliphatic chains (A) or aromatic chains (B) at a concentration of 5.0 μM in DMSO.

p_6-based derivatives **10a**-**10d**, **12a**-**12d**, **15e**-**15g** and **17e**-**17g** in DMSO was all 668 nm while that of chlorin f-based derivatives **20e**, **20g** and reference drug Talaporfin was 665 nm, 665 nm and 664 nm, respectively. Moreover, test compounds **12d**, **15e**, **15g**, **17e** and **17f** possess higher molar absorption coefficient compared with Talaporfin, demonstrating their excellent photophysical properties.

2.3. In vitro HDAC inhibition and cytotoxic potency

The cytotoxic activities of target compounds against A549 and HCT116 cells were measured by CCK-8 assay with Talaporfin and SAHA as reference drugs. As shown in Table 1, dark cytotoxicities (*i.e.* chemotherapy) of most target compounds were comparable

Table 1
HDAC1 inhibition activities and cytotoxicities for lead compounds (**7** and **8**) and their designed dual-mode cytotoxic chlorin-based derivatives (IC_{50}, μM).

Compd.	HDAC1	A549		HCT116	
		Dark toxicity	Light toxicity	Dark toxicity	Light toxicity
SAHA	0.049	1.67	1.70	3.75	3.70
7	NT[a]	15.67	0.30	31.33	0.52
8	NT[a]	15.33	0.92	22.77	1.47
10a	224	0.59	0.18	4.14	0.023
10b	201	3.73	0.31	9.14	0.33
10c	81	3.51	0.30	8.63	0.26
10d	90	2.67	0.23	9.28	0.21
12a	79	0.37	0.13	4.18	0.011
12b	40	1.84	0.22	5.54	0.22
12c	49	1.51	0.18	2.81	0.108
12d	88	1.36	0.12	6.89	0.039
15e	27	0.30	0.06	2.79	0.006
15f	30	1.20	0.17	21.20	0.023
15g	30	0.73	0.24	7.86	0.026
17e	11	0.93	0.13	3.49	0.027
17f	66	1.18	0.32	4.60	0.10
17g	42	1.19	0.23	4.16	0.14
20e	28	9.34	0.90	4.60	0.031
20g	31	4.88	0.78	2.92	0.030
Talaporfin	NT[a]	181	6.21	50.72	2.95

[a] NT: Not tested.

with that of SAHA and far beyond that of their corresponding precursors **7** and **8**, indicating that coupling ZBG of HDACI on lead PSs could remarkably improve direct cytotoxicity without light irradiation. In addition, in the presence of light with a dose of 10 J/cm^2, it could be seen that the photocytotoxicity of all target compounds was much higher than that of Talaporfin. Among them, compound **15e** exhibited the highest dark-toxicity (IC_{50} value: 0.30 μM for A549 cells and 2.79 μM for HCT116 cells) and phototoxicity (IC_{50} value: 0.06 μM for A549 cells and 0.006 μM for HCT116 cells).

The HDAC1 inhibition activities of target compounds were assayed using SAHA as reference drug. As shown in Table 1, the HDAC1 inhibitory activities of target compounds except **10a** and **10b** were moderate (IC_{50} values range: 11–90 μM) and much lower than that of SAHA, which probably lies in that HDAC has several different sub-types and HDAC1 may not be the major target of these compounds. The preliminary structure-activity relationship (SAR) analysis showed that the length and type of the carbon chain linker for target compounds had a great influence on HDAC1 inhibitory activity and ZBG type had little effect on that. Among them, HDAC1 inhibitory activity enhanced with their increasing carbon chain growth, and with about 4 carbon atoms as the best. Moreover, HDAC1 inhibitory activity of aromatic carbon chain linker derivatives was superior to that of aliphatic carbon chain linker derivatives.

It was reported that most benzamide-type HDACIs could selectively inhibit HDAC1, HDAC2, HDAC3, HDAC6, HDAC8 or HDAC10. Since the structure of strongest cytotoxic compound **15e** belongs to benzamide-type, we further determined its inhibitory activity against above subtypes of HDAC except HDAC1 using SAHA as reference drug. As shown in Table 2, **15e** could efficaciously inhibit HDAC2 and 10 (IC_{50} value: 2.65 μM for HDAC2 and 1.90 μM for HDAC10). Interestingly, it was notable that **15e** displayed weak inhibition activities towards HDAC1, HDAC3, HDAC6 and HDAC8, which indicated its selective HDAC inhibition activities.

Table 2
Different subtype HDAC inhibition activities for high active compound **15e** (IC_{50}, μM).

Compd.	HDAC2	HDAC3	HDAC6	HDAC8	HDAC10
15e	2.65	72.10	>100	>100	1.90
SAHA	0.015	0.034	0.018	0.188	0.050

2.4. Cellular uptake

The capability of PS to enter tumor cells is crucial for PDT cytotoxic efficacy. Hence, target compound **15e** at concentration of 0.1 μM uptake in A549 cells were evaluated after 24 h incubation time using Talaporfin at concentration of 1.0 μM as control. As depicted in Fig. 3, the cellular uptake rate of **15e** was 9.0-fold higher than that of Talaporfin, implying that **15e** was more likely to be accumulated in A549 cells compared to Talaporfin.

2.5. ROS level

The light excitation of PSs in the presence of tissue oxygen led to the generation of ROS, which is regarded as the key cytotoxic

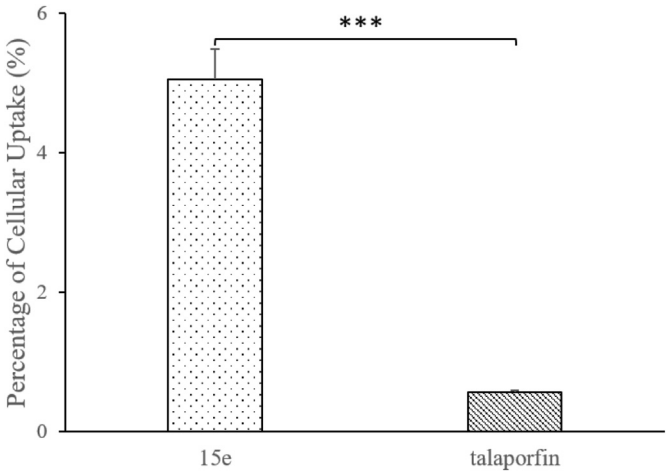

Fig. 3. Cellular uptake rate of compound **15e** (0.1 μM) and Talaporfin (1.0 μM) in A549 cells after 24 h incubation. Statistical analysis by Student's *t*-test: triple asterisks indicate $P < 0.001$ versus negative control.

molecular for causing damage to biological systems [50]. Herein, the intracellular ROS production in A549 cells induced by **15e** and Talaporfin with concentrations of 0.01 μM and 0.05 μM at a light dosage of 10 J/cm^2 were evaluated using 2,7-dichlorodi-hydrofluorescein diacetate (DCFH-DA) as the indicator. DCFH-DA itself was non-fluorescent and its hydrolyzed product (DCF) after interaction with ROS could emit green fluorescent, which could be detected by flow cytometry. As depicted in Fig. 4, compared with negative control (only light irradiation without drug), **15e** could significantly elevate intracellular ROS production under light irradiation, and its mean count value of ROS production was respectively 770.81 for 0.01 μM and 1760.90 for 0.05 μM, which was 6.1 or 11.5 times higher than that of Talaporfin (125.93 for 0.01 μM and 153.14 for 0.05 μM) at the same concentration, probably owing to the higher cellular uptake rate of **15e** compared to Talaporfin and the synergetic effect between PDT and HDACI. Besides, there was significant positive correlation with the concentration in ROS production induced by **15e**.

2.6. Western blotting

To determine whether compound **15e** inhibited the HDAC pathway in cancerous cells, Western blot assay was performed to evaluate its effects on the expression level of acetyl-H3 and acetyl-H4 using SAHA as positive control. A549 cells were exposed to **15e** and SAHA at concentrations of 0.1 μM, 1.0 μM and 2.0 μM for 24 h. As shown in Fig. 5, **15e** could significantly up-regulate Acetyl-H4 levels in a dosage-dependent manner and but almost not affect the expression levels of Acetyl-H3, clearly indicating its inhibition target in A549 cells as a HDACI.

2.7. Subcellular localization

The short life-time of ROS induced by PDT, especially singlet oxygen ($^1O_2$), is the major reason why it is crucial to determine the subcellular localization of the PS, for the intracellular location demonstrates the site of the primary photodamages and the type of cellular response to the therapy. While ROS is short-lived, its intracellular targets for are close to the sites where the PS is located. Hence, cellular structures containing PS would be preferentially damaged upon light irradiation [17,47].

The subcellular localization of **15e** was assessed by laser confocal microscopy upon exposure of A549 cells to **15e** (0.1 μM) in the dark for 24 h. As depicted in Fig. 6, the fluorescence of organelle specific fluorescent probes including Mito Tracker Green (mitochondria, green signal, Fig. 6M3), Lyso Tracker Green DND-26 (lysososomes, green signal, Fig. 6L3), ER Tracker Green (endoplasmic reticulum, green signal, Fig. 6E3) or Golgi Tracker Green (golgi apparatus, green signal, Fig. 6G3) could superimpose well with that of **15e** (red signal, Fig. 6M2, L2, E2 and G2). After entry into cells, **15e** was not observed inside the nucleus of A549 cells.

The merged images revealed the overlaps of **15e** with Mito Tracker Green (yellow signal, Fig. 6M4) or Lyso Tracker Green DND-26 (yellow signal, Fig. 6L4) or ER Tracker Green (yellow signal, Fig. 6E4) or Golgi Tracker Green (yellow signal, Fig. 6G4), indicating that **15e** could be localized in mitochondria, lysosomes, endoplasmic reticulum (ER) and golgi etc. multiple organelles. As a result, the photodynamic damage effect to multiple organelles caused by **15e** presumably could trigger various apoptotic pathways, leading to effective cell destruction [51,52].

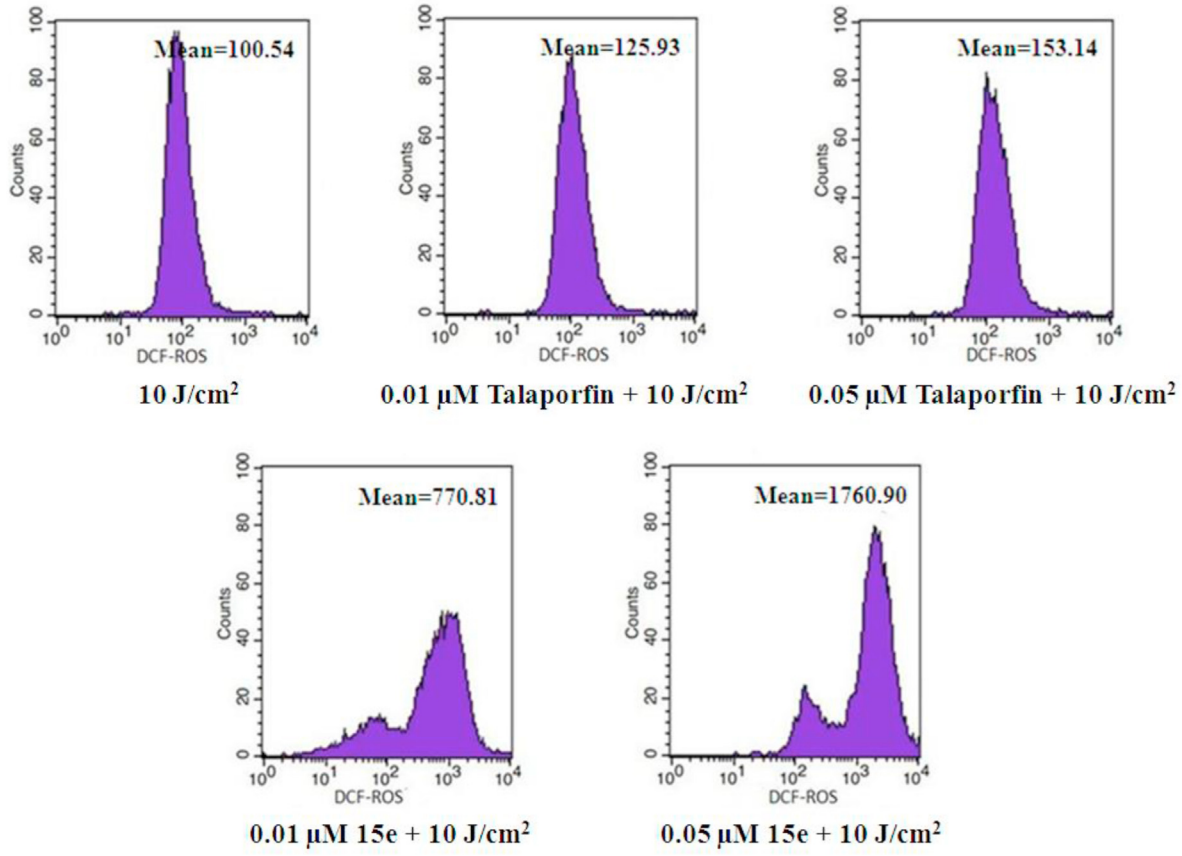

Fig. 4. The ROS production in A549 cells induced by compound **15e** or Talaporfin with light irradiation at a dosage of 10 J/cm^2.

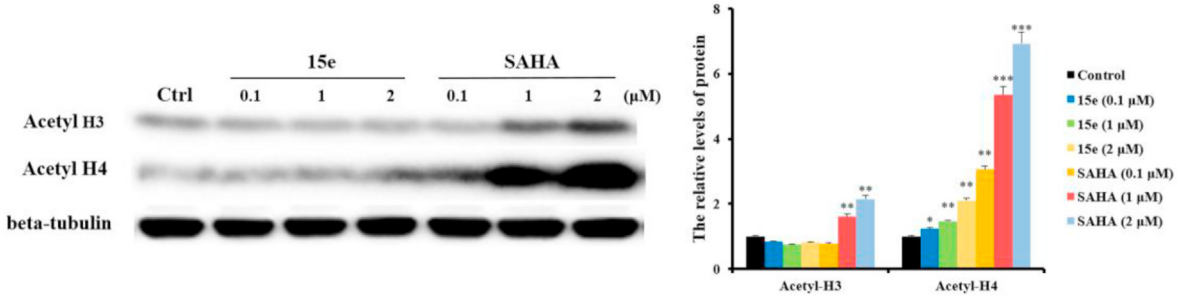

Fig. 5. Western blots showing the levels of acetyl-H3 and acetyl-H4 proteins in A549 cells treated with compound **15e** and SAHA in the dark. Statistical analysis by Student's *t*-test: single asterisks indicate $P < 0.05$, double asterisks indicate $P < 0.01$, and triple asterisks indicate $P < 0.001$ versus negative control.

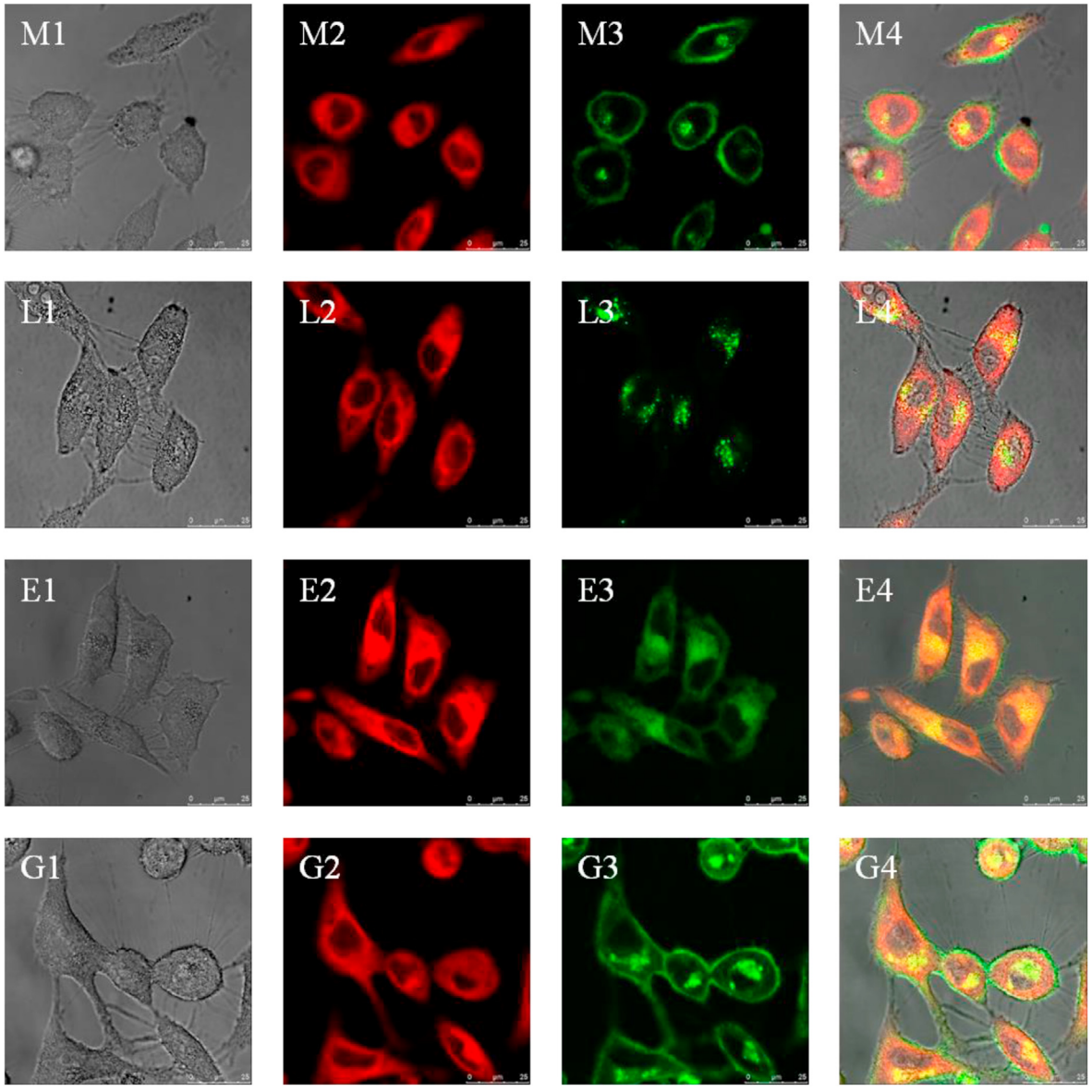

Fig. 6. Intracellular localization of **15e** in A549 cells at 0.1 μM for 24 h: (M1, L1, E1, G1) phase contrast; (M2, L2, E2, G2) initial fluorescence of compound **15e**; (M3) Mitochondria Green Tracker; (L3) Lysosome Green Tracker; (E3) ER Green Tracker; (G3) Golgi Green Tracker; (M4, L4, E4, G4) the overlapped fluorescence of **15e** and organelle Trackers; Scale bar: 10 μm.

2.8. Cell apoptosis

Many excited PSs induced by light generate ROS that lead to induction of apoptosis in malignant cells [53]. Thus, compound **15e** was evaluated to further investigate its effect on inducing cancerous cell apoptosis by Annexin V-FITC/Propidium Iodide (PI) assay, using Talaporfin as reference drug. A549 cells were incubated with vehicle alone or tested samples at various concentrations for 48 h. As shown in Fig. 7, the cells treated by **15e** at a dose of 0.5 μM in the absence of light irradiation were almost all died and the rates of necrosis and apoptosis were respectively 45.22% and 54.74% (Fig. 7A—ii), indicating that **15e** could significantly induce apoptosis of tumor cells as a HDACI (Fig. 7B). In addition, **15e** at low doses of 0.01 μM and 0.1 μM in presence of light irradiation also could significantly bring about induction of apoptosis in a dosage-dependent manner (Fig. 7B) and its percentage of cell apoptosis was individually 27.32% (Fig. 7A-iii) and 90.77% (Fig. 7A—iv), which was significantly higher than that (19.08%) of Talaporfin at equal concentration (0.1 μM) (Fig. 7A—v and Fig. 7B). These results were accordance with the facts that **15e** was localized in apoptosis-related multiple organelles such as mitochondria, lysosomes, golgi apparatus and ER, and its IC_{50} values for dark-toxicity and phototoxicity against A549 cells were individually 0.3 μM and 0.06 μM, which were well below that (6.21 μM) for phototoxicity.

2.9. Cell autophagy

Autophagy is a process of ordered degradation of dysfunctional cytoplasmic components such as organelles and proteins, and lysosomes are considered as the primary organelles for cell autophagy through its wide array of hydrolytic enzymes [54,55]. During the process of autophagy, an isolation membrane forms in the cytosol, composed of double membrane which gradually expands to enfold damaged organelles and aggregated proteins [56]. The membrane closes to form autophagosomes that can be detected by the small fluorescent molecule DAPRed. We performed the experiment using LysoTracker and DAPRed to directly detect lysosome autophagy in A549 cells induced by compound **15e**. As shown in Fig. 8, the lysosomes and autophagosomes stained by LysoTracker and DAPRed respectively were colocalized in A549 cells after treatment with **15e** without light irradiation, indicating that **15e** could induce tumor cell autophagy as a HDACI. Besides, the stronger rosy fluorescence induced by **15e** under light irradiation demonstrated that **15e** could cause tumor cell autophagy to a greater extent as a PS.

3. Conclusions

In summary, this study highlighted an efficient strategy for the combination of PDT and chemotherapy to discover the dual-mode cytotoxic drug by synthesizing a series of chlorin p_6-and chlorin f-based derivatives conjugated to HDACI pharmacophores via aliphatic or aromatic carbon chain linkages. Consequently, dark-toxicity (*i.e.* chemotherapeutic activity) of most target compounds was comparable that of SAHA and far beyond that of their corresponding precursors **7** and **8** while photocytotoxicity (*i.e.* PDT activity) of all target compounds was much higher than that of Talaporfin. In particular, compound **15e** exhibited the highest dark-toxicity and phototoxicity against A549 and HCT116 cells, and was liable to enter A549 cells and localized in mitochondria, lysosomes, golgi and endoplasmic reticulum (ER) etc. multiple organelles, leading to its higher cellular uptake rate, induction of cell apoptosis rate and ROS production compared to Talaporfin. Moreover, **15e** showed definite HDAC2 and 10 inhibitory activities by significantly up-regulating expression of acetyl-H4. Interestingly, **15e** also could induce tumor cell autophagy as a both PS and HDACI. Taken together, all data supported the fact that 15e should be a promising dual-mode cytotoxic drug for PDT and chemotherapy due to its not only much higher PDT cytotoxic efficacy than Talaporfin as a PS but also stronger chemotherapeutic cytotoxicity compared to SAHA as a HDACI. To the best of our knowledge, this is the first example that a single small molecule can play dual-mode cytotoxic effect as a PS and HDACI. Further mechanism, lead-optimization and in vivo antitumor efficacy on tumor-bearing mice studies are in progress.

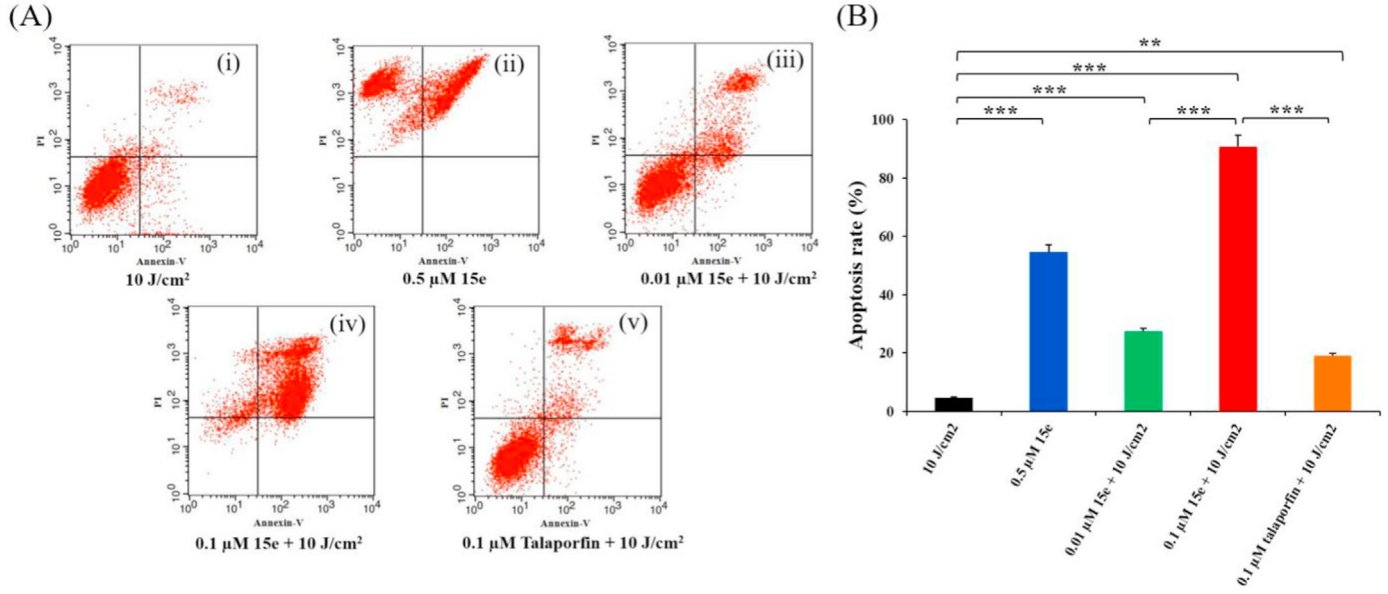

Fig. 7. Flow cytometry analysis of A549 cells with Annexin V-PI double stained after drug administration: (A) Scatter plots showing relative fluorescent intensity for the flow channels following (i) control (only light irradiation), (ii) 0.5 μM of **15e** without light irradiation, (iii) 0.01 μM **15e** at a light dose of 10 J/cm^2, (iv) 0.1 μM **15e** at a light dose of 10 J/cm^2 or (v) 0.1 μM Talaporfin at a light dose of 10 J/cm^2. (B) Bar chart illustrating the apoptosis rate of cells for each of the treatments. Statistical analysis by Student's *t*-test: double asterisks indicate $P < 0.01$, triple asterisks indicate $P < 0.001$.

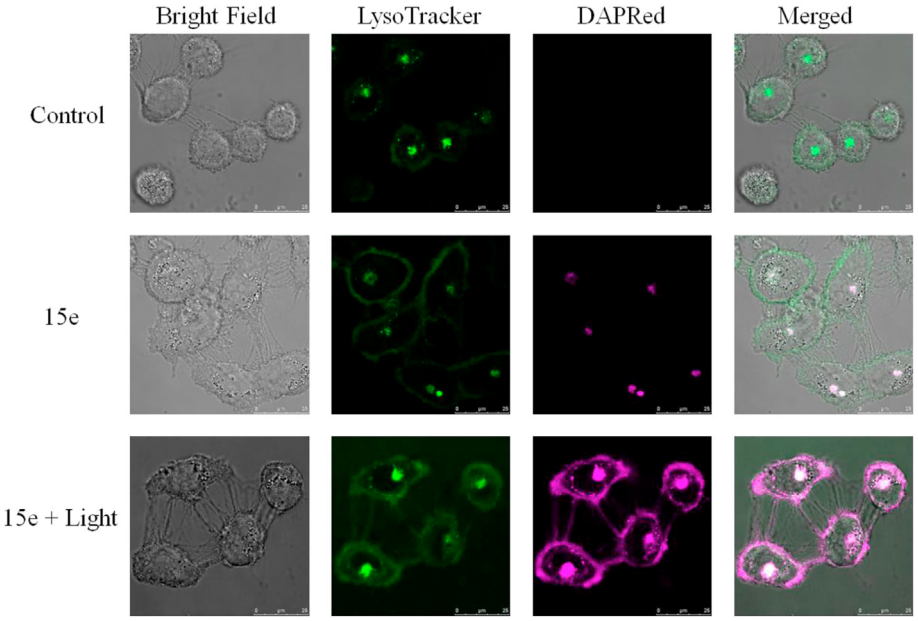

Fig. 8. Cell autophagy in A549 cells induced by compound **15e** at 0.1 μM without or with light irradiation using a laser at 660 nm for a light dose of 1.0 J/cm^2.

4. Materials and methods

4.1. Materials

All chemicals were of reagent grade. All the reagents and solvents were purchased from commercial sources and used without further purification. All oxygen and moisture sensitive reactions were performed in dried solvents under a nitrogen atmosphere. ^{1}H and ^{13}C spectra were recorded on Bruker AVANCE600 or AVANCE300, with TMS as the internal standard and $CDCl_3$ or CD_3OD or $(CD_3)_2SO$ (DMSO-d_6) as solvents. Chemical shift (δ) was expressed in ppm and coupling constants (J) was given in Hz. ESI mass spectrometric data were collected on an API-3000 LC-MS spectrometer or a Micromass Qtof-Micro LC-MS-MS. Thin-layer chromatography (TLC) analysis was carried out on silica gel plates GF254 (QindaoHaiyang Chemical, China). Column chromatography was performed on silica gel H (Qingdao Haiyang Chemical, China) with the indicated solvent systems. Purity of all final compounds was ≥95% as determined by high performance liquid chromatography (HPLC) (Shimadzu LC-10AT) using acetonitrile/H_2O (90:10, volume ratio) as eluent of 1 mL/min on a C18 column (Shimadzu VP-ODS C18, 5 μm, 4.6 mm × 150 mm). UV absorption spectra were measured on a Techcomp UV 1102 spectrophotometers.

4.2. Preparation of compounds

4.2.1. 2-(Chlorin p$_6$-13^1,15^1-dimethylester-17^3-acylamino)-phenylamine (**10a**)

Chlorin p$_6$-13^1,15^1-dimethylester (**7**) (150 mg, 0.246 mmol, 1.0 equiv), which was synthesized as our previously reported [16], was dissolved in anhydrous CH_2Cl_2 (30 mL). HBTU (111.80 mg, 0.295 mmol, 1.2 equiv), DIPEA (128.30 μL, 0.738 mmol, 3.0 equiv) and *o*-phenylenediamine (31.86 mg, 0.295 mmol, 1.2 equiv) were then added and the mixture was allowed to stir for 12 h at room temperature under nitrogen. The reaction solution was washed by 5% citric acid solution (30 mL × 3), saturated NaCl solution and water, and the organic layer was dried over anhydrous Na_2SO_4 and evaporated. The dry residue was purified by column chromatography (CH_2Cl_2: MeOH: HCO_2H = 50 : 1: 0.1) to give 107 mg, 62.2% yield of **10a** ($C_{41}H_{44}N_6O_5$) as a black solid. ^{1}H NMR (Acetone-d_6, 600 MHz): δ 9.81 (s, 1H), 9.55 (s, 1H), 8.98 (s, 1H), 8.39 (s, 1H), 8.10 (dd, J = 17.8, 11.6 Hz, 1H), 7.07 (d, J = 7.74 Hz, 1H), 6.87 (m, 1H), 6.72 (d, J = 7.9 Hz, 1H), 6.54 (t, J = 7.9 Hz, 1H), 6.36 (d, J = 17.9 Hz, 1H), 6.13 (d, J = 11.6 Hz, 1H), 5.23 (m, 1H), 4.68 (q, J = 7.2 Hz, 1H), 4.20 (s, 3H), 4.18 (s, 3H), 3.72 (q, J = 7.7 Hz, 2H), 3.63 (s, 3H), 3.42 (s, 3H), 3.20 (s, 3H), 2.72 (s, 2H), 1.95 (m, 2H), 1.90 (d, J = 7.3 Hz, 3H), 1.66 (t, J = 7.7 Hz, 3H). MS (ESI$^+$) *m/z*: 701.42 [M + H]$^+$ (100%).

4.2.2. 2-[4-(Chlorin p6-131,151-dimethylester-173-acylamino)-butyrylamino]-phenylamine (10b)

7 (150 mg, 0.246 mmol, 1.0 equiv) was dissolved in anhydrous CH_2Cl_2 (30 mL). EDCI (48.51 mg, 0.27 mmol, 1.1 equiv), NHS (31.07 mg, 0.27 mmol, 1.1 equiv) and DMAP (16.47 mg, 0.135 mmol, 0.55 equiv) was then added, and the mixture was stirred for 24 h at room temperature under nitrogen. 4-aminobutyric acid (27.87 mg, 0.27 mmol, 1.1 equiv) and pyridine (1.5 mL) were added and the mixture was continued stirring for 48 h. The reaction solution was washed with 8% HCl (30 mL × 3), saturated NaCl solution and water, and the organic layer was dried over anhydrous Na_2SO_4 and evaporated. The residue was purified by silica gel column chromatography (CH_2Cl_2: MeOH: HCO_2H = 45 : 1: 0.1) to give immediate **9b** (116 mg, yield 67.5%) as a black green solid. **9b** (116 mg, 0.166 mmol, 1.0 equiv), HBTU (75.42 mg, 0.199 mmol, 1.2 equiv), DIPEA (82.15 μL, 0.498 mmol, 3.0 equiv) and *o*-phenylenediamine (21.49 mg, 0.199 mmol, 1.2 equiv) were dissolved in anhydrous CH_2Cl_2 (30 mL), and the mixture was allowed to stir at room temperature for 12 h under nitrogen. The reaction solution was washed by 5% citric acid solution (30 mL × 3), saturated NaCl solution and water, and the organic layer was dried over anhydrous Na_2SO_4 and evaporated. The residue was purified by column chromatography (CH_2Cl_2: MeOH: HCO_2H = 45 : 1: 0.1) to give 88 mg, 45.6% yield of **10b** ($C_{45}H_{51}N_7O_6$) as a black solid. ^{1}H NMR (DMSO-d_6, 300 MHz): δ 9.72 (s, 1H), 9.42 (s, 1H), 9.16 (s, 1H), 8.83 (s, 1H), 7.99 (dd, J = 17.6, 11.6 Hz, 1H), 7.73 (s, 1H), 7.41 (s, 1H), 7.01 (s, 1H), 6.22 (d, J = 17.9 Hz, 1H), 6.03 (d, J = 11.6 Hz, 1H), 4.93 (m, 1H), 4.46 (m, 1H), 4.09 (s, 3H), 4.06 (s, 3H), 3.65 (m, 2H), 3.56 (s, 3H), 3.45 (m, 2H), 3.20 (s, 3H), 3.13 (s, 3H), 2.96 (m, 2H), 2.17 (m, 2H), 1.73 (d, J = 6.7 Hz, 3H), 1.57 (t, J = 6.9 Hz, 5H), 1.40 (m, 2H), 1.16 (m,2H), 0.81 (m, 2H). MS (ESI$^+$) *m/*

z: 786.53 $[M + H]^+$ (100%).

4.2.3. 2-[5-(Chlorin p_6-13^1,15^1-dimethylester-17^3-acylamino)-valerylamino]-phenylamine (**10c**)

According to the similar procedure for the synthesis of **10b**, **7** (150 mg, 0.246 mmol, 1.0 equiv) was reacted with 5-aminovaleric acid (31.59 mg, 0.27 mmol, 1.1 equiv) to afford key immediate **9c**, followed by coupling with *o*-phenylenediamine to obtain 85 mg, 43.2% yield of **10c** ($C_{46}H_{53}N_7O_6$) as a black solid. ^{1}H NMR (DMSO-d_6, 300 MHz): δ 9.70 (s, 1H), 9.65 (s, 1H), 9.41 (s, 1H), 8.87 (s, 1H), 7.99 (dd, J = 17.8, 11.7 Hz, 1H), 7.79 (s, 1H), 7.47 (s, 1H), 7.02 (s, 1H), 6.23 (d, J = 17.9 Hz, 1H), 6.03 (d, J = 11.6 Hz, 1H), 4.93 (m, 1H), 4.51 (m, 1H), 4.10 (s, 3H), 4.08 (s, 3H), 3.62 (m, 2H), 3.56 (s, 3H), 3.24 (m, 3H), 3.12 (s, 3H), 2.27 (m, 2H), 1.75 (d, J = 6.7 Hz, 3H), 1.57 (t, J = 7.3 Hz, 3H), 1.48 (s, 2H), 1.16 (m, 2H), 0.82 (m, 2H). MS (ESI^+) *m/z*: 800.72 $[M + H]^+$(100%).

4.2.4. 2-[6-(Chlorin p_6-13^1,15^1-dimethylester-17^3-acylamino)-hexanoylamino]-phenylamine (**10d**)

According to the similar procedure for the synthesis of **10b**, **7** (150 mg, 0.246 mmol, 1.0 equiv) was reacted with 6-aminocaproic acid (35.37 mg, 0.27 mmol, 1.1 equiv) to afford key immediate **9d**, followed by coupling with *o*-phenylenediamine to obtain 97 mg, 48.5% yield of **10d** ($C_{47}H_{55}N_7O_6$) as a black solid. ^{1}H NMR (DMSO-d_6, 300 MHz): δ 9.77 (s, 1H), 9.59 (s, 1H), 9.19 (s, 1H), 9.01 (s, 1H), 8.22 (dd, J = 17.7, 11.6 Hz, 1H), 7.74 (m, 1H), 7.11 (m, 1H), 6.78 (m, 1H), 6.41 (d, J = 17.3 Hz, 1H), 6.18 (d, J = 11.6 Hz, 1H), 4.97 (m, 1H), 4.54 (m, 1H), 4.14 (s, 3H), 4.11 (s, 3H), 3.72 (m, 2H), 3.59 (s, 3H), 3.44 (s, 3H), 3.20 (s, 3H), 2.26 (m, 2H), 1.81 (d, J = 6.9 Hz, 3H), 1.61 (t, J = 7,2 Hz, 3H), 1.48 (m, 4H), 0.97 (m, 2H), 0.83 (m, 2H). MS (ESI^+) *m/z*: 814.50 $[M + H]^+$(100%).

4.2.5. N-(Chlorin p_6-13^1,15^1-dimethylester-17^3-acyl)-hydroxylamine (**12a**)

7 (150 mg, 0.246 mmol, 1.0 equiv), HATU (112.17 mg, 0.295 mmol, 1.2 equiv) and DIPEA (128.30 μL, 0.738 mmol, 3.0 equiv) were dissolved in anhydrous CH_2Cl_2 (30 mL) and the mixture was stirred for 0.5 h at room temperature. O-tritylhydroxylamine (81.12 mg, 0.295 mmol, 1.2 equiv) was then added, and the mixture was stirred for 24 h. The reaction solution was diluted with CH_2Cl_2 (50 mL) and washed by 5% citric acid solution (30 mL × 2) and saturated NaCl solution (30 mL × 2). The organic layer was dried over anhydrous Na_2SO_4 and evaporated. The residue was purified by column chromatography (CH_2Cl_2: MeOH = 45 : 1) to give key immediate **11a** (121 mg, yield 56.5%) as a black solid. **11a** was dissolved in dried CH_2Cl_2 under ice bath, followed by the addition of $BF_3 \cdot Et_2O$ (0.1 mL) dropwise to react for 2 h. The reaction solution was then diluted with CH_2Cl_2 and washed by saturated NaCl solution (30 mL × 2) and water. The organic layer was dried over anhydrous Na_2SO_4 and evaporated. The residue was purified by column chromatography (CH_2Cl_2: MeOH: HCO_2H = 30 : 1: 0.1) to give 67 mg, 43.6% yield of **12a** ($C_{35}H_{39}N_5O_6$) as a black solid. ^{1}H NMR (Acetone-d_6, 600 MHz): δ 9.86 (s, 1H), 9.62 (s,1H), 9.16 (s, 1H), 8.97 (s, 1H), 8.15 (dd, J = 18.00, 11.70 Hz, 1H), 6.39 (d, J = 17.5 Hz, 1H), 6.15 (d, J = 11.2 Hz, 1H), 5.11 (m, 1H), 4.57 (m, 1H), 4.17 (s, 3H), 4.16 (s, 3H), 3.77 (m, 2H), 3.63 (s, 3H), 3.45 (s, 3H), 3.24 (s, 3H), 3.13 (s, 3H), 2.75 (s, 2H), 2.22 (m, 2H), 1.85 (d, J = 7.0 Hz, 3H), 1.67 (t, J = 7.6 Hz, 5H). MS (ESI^+) *m/z*: 626.27 $[M + H]^+$(100%).

4.2.6. N-[4-(Chlorin p_6-13^1,15^1-dimethylester-17^3-acylamino)]-butyrylhydroxylamine (**12b**)

9b (116 mg, 0.166 mmol, 1.0 equiv), which was prepared according to the similar procedure above, was dissolved in anhydrous CH_2Cl_2 (30 mL). HATU (75.62 mg, 0.199 mmol, 1.2 equiv) and DIPEA (82.15 μL, 0.498 mmol, 3.0 equiv) were then added and the mixture was allowed to stir for 0.5 h at room temperature. O-tritylhydroxylamine (54.72 mg, 0.199 mmol, 1.2 equiv) was added and the mixture was continued stirring for 24 h. The reaction solution was diluted with CH_2Cl_2 (50 mL) and washed by 5% citric acid solution (30 mL × 2) and saturated NaCl solution (30 mL × 2). The organic layer was dried over anhydrous Na_2SO_4 and evaporated to obtain the immediate **11b** as a black solid. **11b** was dissolved in dried CH_2Cl_2 under ice bath, followed by the addition of $BF_3 \cdot Et_2O$ (0.1 mL) dropwise to stir for 2 h. The reaction solution was then diluted with CH_2Cl_2 and washed by saturated NaCl solution (30 mL × 2) and water. The organic layer was dried over anhydrous Na_2SO_4 and evaporated. The residue was purified by column chromatography (CH_2Cl_2: MeOH: HCO_2H = 30 : 1: 0.1) to give 56 mg, 32.1% yield of **12b** ($C_{39}H_{46}N_6O_7$) as a black solid. ^{1}H NMR (DMSO-d_6, 600 MHz): δ 9.80 (s, 1H), 9.62 (s, 1H), 9.02 (s, 1H), 8.23 (dd, J = 17.9, 11.6 Hz, 1H), 7.61 (t, 1H), 6.46 (d, J = 17.8 Hz, 1H), 6.20 (d, J = 11.6 Hz, 1H), 4.98 (m, 1H), 4.55 (m, 1H), 4.16 (s, 3H), 4.13 (s, 3H), 3.74 (m, 2H), 3.62 (s, 3H),3.47 (m, 3H), 3.24 (s, 2H), 3.19 (s, 3H), 2.93 (m, 2H), 2.12 (m, 2H), 1.83 (d, J = 7.3 Hz, 3H), 1.65 (t, J = 7.6 Hz, 3H), 1.41 (m, 2H), 1.23 (m, 2H). MS (ESI^+) *m/z*: 711.37 $[M + H]^+$(100%).

4.2.7. N-[5-(Chlorin p_6-13^1,15^1-dimethylester-17^3-acylamino)]-valerylhydroxylamine (**12c**)

According to the similar procedure for the synthesis of **12b**, **7** (150 mg, 0.246 mmol, 1.0 equiv) was reacted with 5-aminovaleric acid (31.59 mg, 0.27 mmol, 1.1 equiv) to afford key immediate **9c**, followed by coupling with O-tritylhydroxylamine to give crude **11c**. The O-triphenylmethyl protective group of **11c** was finally removed by $BF_3 \cdot Et_2O$ to obtain 52 mg, 29.2% yield of **12c** ($C_{40}H_{48}N_6O_7$) as a black solid. ^{1}H NMR (DMSO-d_6, 600 MHz): δ 9.78 (s, 1H), 9.60 (s, 1H), 9.00 (s, 1H), 8.22 (dd, J = 17.9, 11.58 Hz, 1H), 7.59 (t, 1H), 6.42 (d, J = 17.8 Hz, 1H), 6.18 (d, J = 11.6 Hz, 1H), 4.97 (m, 1H), 4.54 (m, 1H), 4.14 (s, 3H), 4.11 (s, 3H), 3.73 (m, 2H), 3.60 (s, 3H), 3.45 (m, 3H), 3.22 (s, 2H), 3.17 (s, 3H), 2.90 (m, 2H), 2.10 (m, 4H), 1.82 (d, J = 7.3 Hz, 3H), 1.63 (t, J = 7.6 Hz, 3H), 1.40 (m, 2H), 1.34 (m, 2H). MS (ESI^+) *m/z*: 725.36 $[M + H]^+$(100%).

4.2.8. N-[6-(Chlorin p_6-13^1,15^1-dimethylester-17^3-acylamino)]-hexanoylhydroxylamine (**12d**)

According to the similar procedure for the synthesis of **12b**, **7** (150 mg, 0.246 mmol, 1.0 equiv) was reacted with 6-aminocaproic acid (35.37 mg, 0.27 mmol, 1.1 equiv) to afford key immediate **9d**, followed by coupling with O-tritylhydroxylamine to give crude **11d**. The O-triphenylmethyl protective group of **11d** was finally removed by $BF_3 \cdot Et_2O$ to obtain 61 mg, 33.6% yield of **12d** ($C_{41}H_{50}N_6O_7$) as a black solid. ^{1}H NMR (DMSO-d_6, 600 MHz): δ 10.24 (s, 1H), 9.76 (s, 1H),9.57 (s, 1H), 9.00 (s, 1H), 8.61 (s, 1H), 8.19 (dd, J = 17.8, 11.5 Hz, 1H), 7.67 (t, 1H), 6.41 (d, J = 17.8 Hz, 1H), 6.17 (d, J = 11.40 Hz, 1H), 5.75 (s, 2H), 4.97 (m, 1H), 4.54 (m, 1H), 4.15 (s, 3H), 4.12 (s, 3H), 3.70 (m, 2H), 3.59 (s, 3H), 3.44 (s, 3H), 3.26 (m, 2H), 3.19 (s, 3H), 2.92 (m, 2H), 2.11 (m, 2H), 1.85 (m, 2H), 1.83 (d, J = 7.3 Hz, 3H), 1.61 (t, J = 7.6 Hz, 3H), 1.51 (m, 2H), 1.40 (m, 2H),1.25 (m, 2H). MS (ESI^+) *m/z*: 739.51 $[M + H]^+$(100%).

4.2.9. 4-(Chlorin p_6-13^1,15^1-dimethylester-17^3-acylamino)-N-(2-aminophenyl)-benzamide (**15e**)

To a solution of compound **7** (150 mg, 0.246 mmol, 1.0 equiv) in dried CH_2Cl_2, HATU (112.17 mg, 0.295 mmol, 1.2 equiv), DIPEA (128.30 μL, 0.738 mmol, 3.0 equiv) and 4-aminobenzoic acid *tert*-butyl ester (52.11 mg, 0.270 mmol, 1.1 equiv) were then added, and the mixture was stirred for 48 h at room temperature. The reaction solution was successively washed with 8% HCl (30 mL × 3), saturated NaCl solution and water. The organic layer was dried over anhydrous Na_2SO_4 and evaporated to give immediate **13e** as a black solid. **13e** was dissolved in dry CH_2Cl_2/TFA (1:1, 10 mL) and stirred

for 4 h under ice bath. The resulting mixture was diluted with CH_2Cl_2 and adjusted to pH 3–4 with 10% $NaHCO_3$ solution. The residue was purified by silica gel column chromatography (CH_2Cl_2: MeOH: HCO_2H = 45:1:0.1) to afford key immediate **14e** (113 mg, yield 63.1%) as a black green solid. **14e** (113 mg, 0.155 mmol, 1.0 equiv), HBTU (70.49 mg, 0.186 mmol, 1.2 equiv), DIPEA (76.90 μL, 0.465 mmol, 3.0 equiv) and *o*-phenylenediamine (20.08 mg, 0.186 mmol, 1.2 equiv) were dissolved in anhydrous CH_2Cl_2 (30 mL), and the mixture was allowed to stir for 12 h at room temperature under nitrogen. The reaction solution was washed by 5% citric acid solution (30 mL × 3), saturated NaCl solution and water. The organic layer was dried over anhydrous Na_2SO_4 and evaporated. The residue was purified by column chromatography (CH_2Cl_2: MeOH = 50 : 1) to give 83 mg, 41.2% yield of **15e** ($C_{48}H_{49}N_7O_6$) as a black solid. ^{1}H NMR (Acetone-d_6, 600 MHz): δ 9.86 (s, 1H), 9.63 (s, 1H), 8.93 (s, 1H), 8.69 (s, 1H), 8.14 (dd, *J* = 17.8, 11.5 Hz, 1H), 7.81 (m, 2H), 7.37 (m, 2H),7.26 (m, 1H), 6.96 (m, 1H), 6.83 (m, 1H), 6.64 (m, 1H), 6.38 (d, *J* = 18.00 Hz, 1H), 6.15 (d, *J* = 11.8 Hz, 1H), 5.23 (m, 1H), 4.64 (m, 1H), 4.18 (s, 3H), 4.15 (s, 3H), 3.78 (m, 2H), 3.63 (s, 3H), 3.38 (s, 3H), 3.25 (s, 3H), 2.75 (s, 2H), 2.13 (m, 2H), 1.87 (d, *J* = 7.3 Hz, 3H), 1.68 (t, *J* = 7.6 Hz, 3H). ^{13}C NMR (Acetone-d_6, 600 MHz): δ170.14, 166.40, 145.02, 128.78, 128.24, 127.50, 123.98, 121.69, 121.66, 119.55, 118.16, 118.02, 117.39, 104.14, 99.69, 93.87, 52.91, 52.88, 52.27, 51.59, 49.07, 31.16, 29.45, 29.33, 29.21, 29.08, 28.95, 28.82, 28.69, 28.57, 23.14, 18.74, 16.99, 11.48, 11.15, 10.06. MS (ESI$^+$) *m/z*: 820.49 [M + H]$^+$(100%). HRMS (ESI$^+$) *m/z*: 820.3817 [M+H]$^+$, calcd for $C_{48}H_{49}N_7O_6$ 819.3744. HPLC purity: 99.1%.

*4.2.10. 3-(Chlorin p_6-13^1,15^1-dimethylester-17^3-acylamino)-N-(2-aminophenyl)-cinnamamide (**15f**)*

According to the similar procedure for the synthesis of **15e**, **7** (150 mg, 0.246 mmol, 1.0 equiv) was reacted with 3-aminocinnamic acid *tert*-butyl ester (59.13 mg, 0.27 mmol, 1.1 equiv) to afford immediate **13f**. The *tert*-butyl protective group of compound **13f** was removed by TFA to give **14f**, followed by coupling with *o*-phenylenediamine to obtain 82 mg, 39.4% yield of **15f** ($C_{50}H_{51}N_7O_6$) as a black solid. ^{1}H NMR (Acetone-d_6, 600 MHz): δ 9.86 (s, 1H), 9.62 (s, 1H), 8.92 (s, 1H), 8.51 (m, 1H), 8.18 (dd, *J* = 17.5, 11.3 Hz, 1H), 8.12 (m, 1H), 7.51 (t, 1H), 7.35 (m, 2H), 7.27 (m, 2H), 7.03 (m, 1H), 6.88 (m, 1H), 6.76 (m, 1H), 6.65 (m, 1H), 6.38 (d, *J* = 17.9 Hz, 1H), 6.16 (d, *J* = 11.6 Hz, 1H), 5.24 (m, 1H), 4.64 (m, 1H), 4.18 (s, 3H), 4.15 (s, 3H), 3.78 (m, 2H), 3.64 (s, 3H),3.36 (s, 3H), 3.25 (s, 3H), 2.06 (m, 2H), 1.95 (m, 2H), 1.87 (d, *J* = 7.3 Hz, 3H), 1.68 (t, *J* = 7.7 Hz, 3H). MS (ESI$^+$) *m/z*: 846.31 [M + H]$^+$(100%).

*4.2.11. 4-(Chlorin p_6-13^1,15^1-dimethylester-17^3-acylamino)-N-(2-aminophenyl)-cinnamamide (**15g**)*

According to the similar procedure for the synthesis of **15e**, **7** (150 mg, 0.246 mmol, 1.0 equiv) was reacted with 4-aminocinnamic acid *tert*-butyl ester (59.13 mg, 0.27 mmol, 1.1 equiv) to afford immediate **13g**. The *tert*-butyl protective group of **13g** was removed by TFA to give **14g**, followed by coupling with *o*-phenylenediamine to obtain 85 mg, 40.9% yield of **15g** ($C_{50}H_{51}N_7O_6$) as a black solid. ^{1}H NMR (Acetone-d_6, 600 MHz): δ 9.93 (s, 1H), 9.70 (s, 1H), 8.97 (s, 1H), 8.37 (m, 1H), 8.21 (dd, *J* = 17.7, 11.4 Hz, 1H), 7.56 (m, 1H), 7.39 (m, 4H), 7.08 (m, 1H), 6.97 (m, 1H), 6.84 (m, 1H), 6.70 (m, 1H), 6.43 (d, *J* = 17.9 Hz, 1H), 6.16 (d, *J* = 10.6 Hz, 1H), 5.28 (m, 1H), 4.70 (m, 1H), 4.22 (s, 3H), 4.20 (s, 3H), 3.85 (m, 2H), 3.68 (s, 3H),3.41 (s, 3H), 3.32 (s, 3H), 2.09 (m, 2H), 2,05 (m, 2H), 1.91 (d, *J* = 7.3 Hz, 3H), 1.74 (t, *J* = 7.7 Hz, 3H). MS (ESI$^+$) *m/z*: 846.52 [M + H]$^+$(100%).

*4.2.12. 4-(Chlorin p_6-13^1,15^1-dimethylester-17^3-acylamino)-N-hydroxylbenzamide (**17e**)*

To a solution of compound **7** (150 mg, 0.246 mmol, 1.0 equiv) in dried CH_2Cl_2, HATU (112.17 mg, 0.295 mmol, 1.2 equiv), DIPEA (128.30 μL, 0.738 mmol, 3.0 equiv) and 4-aminobenzoic acid *tert*-butyl ester (52.11 mg, 0.270 mmol, 1.1 equiv) was then added. After stirring for 48 h, the reaction mixture was washed with 8% HCl (30 mL × 3), saturated NaCl solution and water. The organic layer was dried over anhydrous Na_2SO_4 and evaporated to give the immediate **13e** as a black solid. **13e** was dissolved in dry CH_2Cl_2/TFA (1:1, 10 mL) and stirred for 4 h under ice bath. The resulting mixture was diluted with CH_2Cl_2 and adjusted to pH 3–4 with 10% $NaHCO_3$ solution. The residue was purified by silica gel column chromatography (CH_2Cl_2: MeOH: HCO_2H = 45 : 1: 0.1) to afford key immediate **14e** (108 mg, yield 59.8%) as a black green solid. **14e** (108 mg, 0.147 mmol, 1.0 equiv), HATU (67.03 mg, 0.176 mmol, 1.2 equiv) and DIPEA (72.90 μL, 0.441 mmol, 3.0 equiv) were dissolved in anhydrous CH_2Cl_2 (30 mL), and the mixture was allowed to stir for 0.5 h at room temperature. O-tritylhydroxylamine (48.39 mg, 0.176 mmol, 1.2 equiv) was then added and the mixture was continued stirring for 24 h. The reaction solution was diluted with CH_2Cl_2 (50 mL) and washed by 5% citric acid solution (30 mL × 2) and saturated NaCl solution (30 mL × 2). The organic layer was dried over anhydrous Na_2SO_4 and evaporated to obtain immediate **16e** as a black solid. **16e** was dissolved in dried CH_2Cl_2 under ice bath, followed by the addition of $BF_3 \cdot Et_2O$ (0.1 mL) dropwise to stir for 2 h. The mixture solution was then diluted with CH_2Cl_2 and washed by saturated NaCl solution (30 mL × 2) and water. The organic layer was dried over anhydrous Na_2SO_4 and evaporated. The residue was purified by column chromatography (CH_2Cl_2: MeOH: HCO_2H = 30:1:0.1) to obtain 57 mg, 31.1% yield of **17e** ($C_{42}H_{44}N_6O_7$) as a black solid. ^{1}H NMR (Acetone-d_6, 600 MHz): δ 10.59 (s, 1H), 9.88 (s, 1H), 9.65 (s, 1H), 8.95 (s, 1H), 8.16 (dd, *J* = 17.3, 11.5 Hz, 1H), 7.62 (t, 2H), 7.37 (t, 2H), 6.40 (d, *J* = 18.30 Hz, 1H), 6.18 (d, *J* = 10.4 Hz, 1H), 5.62 (s, 1H), 4.64 (m, 1H), 4.19 (s, 3H), 4.15 (s, 3H), 3.80 (m, 2H), 3.65 (s, 3H), 3.39 (s, 3H), 3.27 (s, 3H), 2.50 (m, 2H), 2.16 (m, 2H), 1.88 (d, *J* = 4.7 Hz, 3H), 1.69 (t, *J* = 7.2 Hz, 3H). MS (ESI$^+$) *m/z*: 745.48 [M + H]$^+$(100%).

*4.2.13. 3-(Chlorin p_6-13^1,15^1-dimethylester-17^3-acylamino)-N-hydroxylcinnamamide (**17f**)*

According to the similar procedure for the synthesis of **17e**, **7** (150 mg, 0.246 mmol, 1.0 equiv) was reacted with 3-aminocinnamic acid *tert*-butyl ester (59.13 mg, 0.27 mmol, 1.1 equiv) to obtain immediate **13f**. The *tert*-butyl protective group of compound **13f** was removed by TFA to give crude **14f**. **14f** was reacted with O-tritylhydroxylamine to get immediate **16f**, followed by the deprotection of O-triphenylmethyl group by $BF_3 \cdot Et_2O$ to obtain 55 mg, 29.0% yield of **17f** ($C_{44}H_{46}N_6O_7$) as a black solid. ^{1}H NMR (Acetone-d_6, 600 MHz): δ 9.91 (s, 1H), 9.68 (s, 1H), 8.96 (s, 1H), 8.63 (m, 1H), 8.19 (dd, *J* = 18.00, 11.5 Hz, 1H), 7.49 (m, 1H), 7.33 (m, 4H), 6.43 (d, *J* = 17.6 Hz, 1H), 6.20 (d, *J* = 11.3 Hz, 1H), 5.27 (m, 1H), 4.67 (m, 1H), 4.18 (s, 3H), 4.15 (s, 3H), 3.78 (m, 2H), 3.64 (s, 3H), 3.36 (s, 3H), 3.25 (s, 3H), 2.06 (m, 2H), 1.95 (m, 2H), 1.87 (d, *J* = 7.3 Hz, 3H), 1.68 (t, *J* = 7.7 Hz, 3H). MS (ESI$^+$) *m/z*: 771.26 [M + H]$^+$(100%).

*4.2.14. 4-(Chlorin p_6-13^1,15^1-dimethylester-17^3-acylamino)- N-Hydroxylcinnamamide (**17g**)*

According to the similar procedure for the synthesis of **17e**, **7** (150 mg, 0.246 mmol, 1.0 equiv) was reacted with 4-aminocinnamic acid *tert*-butyl ester (59.13 mg, 0.27 mmol, 1.1 equiv) to get immediate **13g**. The *tert*-butyl protective group of compound **13g** was removed by TFA to give crude **14g**. **14g** was reacted with O-tritylhydroxylamine to get immediate **16g**, followed by the deprotection of O-triphenylmethyl group by $BF_3 \cdot Et_2O$ to obtain 58 mg, 30.6% yield of **17g** ($C_{44}H_{46}N_6O_7$) as a black solid. ^{1}H NMR (Acetone-d_6, 600 MHz)δ 9.90 (s, 1H), 9.68 (s, 1H), 9.54 (s, 1H), 9.34 (m, 1H), 8.19 (dd, *J* = 17.4, 11.6 Hz, 1H), 7.45 (m, 1H), 7.31 (m, 2H), 7.20 (m, 2H), 6.41 (d, *J* = 18.3 Hz, 1H), 6.19 (d, *J* = 11.0 Hz, 1H), 5.01

(m, 1H), 4.67 (m, 1H), 4.20 (s, 3H), 4.16 (s, 3H), 3.83 (m, 2H), 3.66 (s, 3H), 3.40 (s, 3H), 3.26 (s, 3H), 2.07 (m, 2H), 1.95 (m, 2H), 1.88 (d, J = 6.1 Hz, 3H), 1.72 (t, J = 7.7 Hz, 3H). MS (ESI^+) *m/z*: 771.43 $[M + H]^+$(100%).

4.2.15. 4-(Chlorin f-13^1-monomethylester-17^3-acylamino)-N-hydroxylbenzamide (**20e**)

Chlorin f (**5**) (650 mg, 1.208 mmol), which was synthesized as our previously reported [49], was dissolved in THF (50 mL). 2.5% CH_2N_2 in Et_2O (10 mL) was added and the mixture was allowed to stir for 10 min under ice bath. Acetic acid (0.2 mL) was then added to decompose excessive CH_2N_2. After removal of solvents of two-thirds volume, the reaction solution was diluted with CH_2Cl_2 (50 mL) and washed with saturated NaCl solution and water. The organic layer was dried over anhydrous Na_2SO_4 and evaporated. The residue was dissolved in THF (100 mL) with addition of 25% HCl (100 mL). The mixture was stirred for 4 h at room temperature and diluted with water, adjusted to pH 5–6 with 1M NaOH, and then extracted with CH_2Cl_2. The organic layer was washed with water, dried over anhydrous Na_2SO_4, and evaporated. The residue was purified on a silica gel column chromatography (CH_2Cl_2: MeOH = 33 : 1) to afford chlorin f-13^1-monomethyl ester (**8**) (405 mg, yield 60.8%) as a black solid. **8** (100 mg, 0.181 mmol, 1.0 equiv), HATU (82.46 mg, 0.217 mmol, 1.2 equiv), DIPEA (94.40 μL, 0.543 mmol, 3.0 equiv) and 4-aminobenzoic acid *tert*-butyl ester (52.11 mg, 0.181 mmol, 1.1 equiv) were dissolved in anhydrous CH_2Cl_2 (30 mL) and the mixture was allowed to stir for 48 h at room temperature under nitrogen. The reaction mixture was washed with 8% HCl (30 mL × 3), saturated NaCl solution and water. The organic layer was dried over anhydrous Na_2SO_4 and evaporated to give the immediate **18e** as a black solid. **18e** was dissolved in dry CH_2Cl_2/TFA (1:1, 10 mL) and stirred for 4 h under ice bath. The resulting mixture was diluted with CH_2Cl_2 and adjusted to pH 3–4 with 10% $NaHCO_3$ solution. The residue was purified by silica gel column chromatography (CH_2Cl_2: MeOH: HCO_2H = 45 : 1: 0.1) to afford key immediate **19e** (78 mg, yield 64.1%) as a black green solid. **19e** (78 mg, 0.116 mmol, 1.0 equiv), HATU (52.90 mg, 0.139 mmol, 1.2 equiv) and DIPEA (57.55 μL, 0.348 mmol, 3.0 equiv) were dissolved in anhydrous CH_2Cl_2 (30 mL), and the mixture was allowed to stir for 0.5 h at room temperature. O-tritylhydroxylamine (38.22 mg, 0.139 mmol, 1.2 equiv) was then added and the mixture was continued stirring for 24 h. The reaction solution was diluted with CH_2Cl_2 (50 mL) and washed by 5% citric acid solution (30 mL × 2) and saturated NaCl solution (30 mL × 2). The organic layer was dried over anhydrous Na_2SO_4 and evaporated. The residue was dissolved in dried CH_2Cl_2 under ice bath, followed by the addition of $BF_3 \cdot Et_2O$ (0.1 mL) dropwise to stir for 2 h. The mixture solution was then diluted with CH_2Cl_2 and washed by saturated NaCl solution (30 mL × 2) and water. The organic layer was dried over anhydrous Na_2SO_4 and evaporated. The residue was purified by column chromatography (CH_2Cl_2: MeOH: HCO_2H = 30 : 1: 0.1) to obtain 51 mg, 41.0% yield of **20e** ($C_{40}H_{42}N_6O_5$) as a black solid. ^{1}H NMR (DMSO-d_6, 600 MHz): δ 10.65 (s, 1H), 9.92 (s, 1H), 9.86 (s, 1H), 9.79 (s, 1H), 9.71 (s, 1H), 9.05 (s, 1H), 8.31 (dd, J = 17.3, 11.3 Hz, 1H), 7.51 (m, 2H), 7.41 (m, 2H), 6.47 (d, J = 17.3 Hz, 1H), 6.18 (d, J = 12.2 Hz, 1H), 4.65 (m, 1H), 4.51 (m, 1H), 4.28 (s, 3H), 3.80 (m, 5H), 3.49 (s, 3H), 3.28 (s, 3H), 1.90 (d, J = 7.1 Hz, 3H), 1.67 (t, J = 7. 6 Hz, 3H). MS (ESI^+) *m/z*: 687.43 $[M + H]^+$(100%).

4.2.16. 4-(Chlorin f-13^1-monomethylester-17^3-acylamino)-N-hydroxylcinnamamide (**20g**)

According to the similar procedure for the synthesis of **20e**, **8** (100 mg, 0.181 mmol, 1.0 equiv) was reacted with 4-aminocinnamic acid *tert*-butyl ester (43.60 mg, 0.199 mmol, 1.1 equiv) to obtain crude product **18g**, followed by coupling with O-tritylhydroxylamine to give immediate **19g**. The O-triphenylmethyl group of compound **19g** was finally removed by $BF_3 \cdot Et_2O$ to obtain 52 mg, 40.4% yield of **20g** ($C_{42}H_{44}N_6O_5$) as a black solid. ^{1}H NMR (DMSO-d_6,600 MHz): δ 11.01 (s, 1H), 9.96 (s, 1H), 9.84 (s, 1H), 9.76 (s, 1H), 9.69 (s,1H), 9.02 (s,1H), 8.85 (s,1H), 8.28 (dd, J = 17.9, 11.5 Hz, 1H), 7.61 (m, 2H), 7.52 (m, 2H), 6.42 (d, J = 18.00 Hz, 1H), 6.19 (d, J = 11.9 Hz, 1H), 4.62 (m, 1H), 4.50 (m, 1H), 4.25 (s, 3H), 3.77 (m, 5H), 3.47 (s, 3H), 3.28 (s, 3H), 2.15 (m, 2H), 1.87 (d, J = 7.2 Hz, 3H), 1.72 (t, J = 7.7 Hz, 3H). MS (ESI^+) *m/z*: 713.61 $[M + H]^+$(100%).

4.3. Photophysical properties

The UV absorption spectra of test compounds with a concentration of 5.0 μM in DMSO were recorded with the UV spectrophotometer (Techcomp UV 1102) at wavelengths from 400 nm to 700 nm. All the measurements were carried out at room temperature.

4.4. In vitro HDAC inhibition assay

The HDAC1 (no. ab101661) was purchased from Abcam, and HDAC2 (H84-30G-10), HDAC3 (H85-30G-10), HDAC6 (H88-30G-10), HDAC8 (H90–30H-10), and HDAC10 (H92-31G-10) were all purchased from Signalchem. The in vitro HDAC inhibition assay for target compounds was performed according to the manufacturer's protocols. The reaction mixture contained 25 mM Tris (pH 8.0), 1 mM $MgCl_2$, 0.1 mg/mL BSA, 137 mM NaCl, 2.7 mM KCl and HDAC (7.2 ng/well) in a total volume of 40 μL. Test compounds (3-fold dilution) were diluted in 10% DMSO, and 5 μL of the dilution was added and pre-incubated with purified recombinant HDAC for 5 min at room temperature before substrate addition. Afterwards, the enzyme substrate (10 μM Ac-Leu-Gly-Lys(Ac)-AMC) was added and the plate was incubated at 37 °C for 30 min in a final volume of 50 μL. Finally, the reaction was quenched with 50 μL of HDAC assay developer (1 mg/mL trypsin and 2 μM TSA in assay buffer) for 30 min at room temperature, and the fluorescence intensity was measured using the Spectra Max M5 microtiter plate reader at excitation and emission wavelengths of 360 nm and 460 nm, respectively. The IC_{50} values were calculated from the fluorescence intensity readings of test wells relative to those of control wells and determined by GraphPad Prism 7.0 for windows software, using the "log (inhibitor) vs normalized response-variable slope" function.

4.5. Cell lines and culture

Human non small cell carcinoma cell line A549 and human colon carcinoma cell line HCT116 were initially purchased from the Chinese Academy of Science Shanghai Institute of Cell Bank (Shanghai, China). All cell lines were cultured in DMEM medium (Hyclone, Logan, UT, USA), which was supplemented with 10% fetal bovine serum (FBS) and 1% Penicillin-Streptomycin solution. The cells were grown as monolayers in sterile, vented-capped, angle-necked cell culture flasks and were maintained in 5% CO_2 in a humidified incubator at 37 °C until confluent.

4.6. Dark toxicity

A stock solution (30 mM) of test compounds was prepared by dissolving compounds in DMSO. The stock solution was serially diluted to different concentrations with the culture medium for cytotoxicity assay. 5×10^3 A549 or HCT116 cells were seeded on 96-well transparent plates and cultured in DMEM media for 24 h. After suction media, the cells were then incubated with fresh medium containing tested compounds with varied concentrations in the dark for 48 h. After the media was removed, the cells were fed with

fresh medum, following 10 μL of Cell Counting Kit-8 (CCK-8) per 100 μL of medium and incubated for another 1.0 h. Cell viability was assessed by Cell-Counting Kit-8 assay (Dojindo Laboratories, Japan) according to the manufacturers' protocol. The absorbance of each well was measured by a spectrophotometer (Tecan, Switzerland) at 450 nm [17].

4.7. Phototoxicity

Cells were prepared as described above and incubated with test compounds of different concentrations for 24 h. After irradiation with the diode laser at 660 nm for a light dose of 10 J/cm2, cells were incubated for another 24 h. Cell viability was then measured as described above using CCK-8 assay [17].

4.8. Cellular uptake

A549 cells were seeded on 6-well transparent plates at the density of 2×10^5 cells (2.0 mL) per well and incubated in a 5% CO_2 incubator at 37 °C for 24 h. The culture medium was then removed, and washed three times by PBS. Cells were then incubated with 0.1 μM of **15e** or 1.0 μM of Talaporfin in fresh medium for 24 h in the dark. After incubation, the cells were rinsed with PBS three times and lysed with 90 μL 1% Triton x-100 in PBS per well. The cell lysates were centrifuged at 12000 g/min for 5 min to obtain the supernatant at 4 °C. The amount of **15e** and Talaporfin was fluorometrically determined with an excitation wavelength of 400 nm and an emission wavelength of 660 nm using a Fluorescence Spectrophotometer (F7000, Hitachi). Quantification of **15e** and Talaporfin was carried out using fluorescence-drug concentration calibration curves generated with their various known concentrations. The cellular uptake rate for drug was then calculated.

4.9. ROS level

3×10^5 A549 cells in 2 mL of culture medium (per well) were seeded on 6-well plates and incubated for 24 h in a 5% CO_2 incubator at 37 °C. The culture medium was removed, and cells were continued to be incubated in fresh medium in presence or absence of 0.01 μM or 0.05 μM of **15e** or Talaporfin in the dark for 24 h. On the basis a standard ROS assay kit instruction, 10 mM 2,7-Dichlorodi-hydrofluorescein diacetate (DCFH-DA) probe was added (2 μL per well) and cells were incubated for another 1 h. The culture medium was refreshed and cells were exposed to the laser at 660 nm for a light dose of 10 J/cm^2. After keeping in the dark for 1 h, cells were collected and analyzed by a flow cytometer (BD Accuri C6).

4.10. Western blotting

A549 cells were seeded (2×10^5 cells per well) on 6-well transparent plates (Corning). The cells were exposed to compound **15e** and SAHA at 0.1, 1.0, and 2 μM for 24 h and then harvested and washed with PBS three times. Then the cells were lysed with RIPA cell lysis buffer for 30 min. The cell lysates were centrifuged at 12000g for 15 min at 4 °C. Supernatant was collected, and BCA protein assay was used for determined protein concentration. Above total protein lysates (20 μg) were separated by 15% sodium dodecyl sulfate polyacrylamide gel electrophoresis (SDS-PAGE) and next transferred to a polyvinylidene fluoride membrane at 100 mA for 2 h. The filter was blocked for 2 h with 5% nonfat dry milk solution in TBST 0.1% Tween (Sigma-Aldrich, Italy) at room temperature. Membranes were incubated with primary antibodies overnight at 4 °C and washed with a 5% nonfat dry milk solution in TBST 0.1% Tween-20 three times and subsequently incubated with corresponding secondary antibodies in the dark for 2 h at room temperature. Target proteins were detected using Odyssey infrared imaging system (Licor, USA). The antibodies including anti-histone H3 (no. ab32356), anti-histone H4 (no. ab51997), and anti-β-tubulin (no. ab52623) were purchased from Abcam.

4.11. Subcellular localization

Approximately 3×10^4 A549 cells were seeded on a cell culture dish (diameter = 35 mm) and incubated in the dark in a 5% CO_2 incubator at 37 °C for 24 h. The medium was replaced by fresh medium containing 0.1 μM **15e** and the cells were incubated for another 24 h. Cells were rinsed with PBS three times and incubated with Mito-Tracker Green probe (Shanghai Beyotime Biotechnology co., Ltd., China) (300 nM) or ER-Tracker Green probe (Shanghai Yeasen Biotechnologies co., Ltd., China) (300 nM) or Golgi-Tracker Green probe (Jiangsu KeyGEN BioTECH co., Ltd., Nanjing, China) (2 μM) for 1 h, or Lyso-Tracker Green DND-26 probe (Shanghai Yeasen Biotechnologies co., Ltd., China) (100 nM) for 1.5 h. Then cells were rinsed with PBS three times again and examined using a Leica TCS SP5 spectral confocal microscope equipped with Argon-Heli-umNenon (Ar-HeNe) laser. Mito-Tracker, Lyso-Tracker, ER-Tracker, Golgi-Tracker and compound **15e** were respectively excited at the wavelength of 488, 488, 488, 488, 405 nm and the signals from different probes were acquired in a sequential scan mode.

4.12. Cell apoptosis

2×10^5 A549 cells in 2 mL of culture medium (per well) were seeded on 6-well transparent plates and incubated for 24 h in a 5% CO_2 incubator at 37 °C. The culture medium was removed, and cells were incubated with **15e** (0.5, 0.1, 0.01 μM) or Talaporfin (0.1, 0.01 μM) in fresh medium in the dark. After 24 h, only the cells treated with **15e** (0.1, 0.01 μM) or Talaporfin (0.1, 0.01 μM) were exposed to the laser at 660 nm for a light dose of 10 J/cm^2 and all the cells were then incubated in a 5% CO_2 incubator at 37 °C for another 24 h in the dark. The cells were then harvested by trypsinization and washed twice with PBS. After centrifugation and removal of the supernatants, the residues were resuspended in 400 μL of 1 × binding buffer, followed by adding 5 μL of Annexin V-FITC, and incubated at room temperature for 15 min. After adding 10 μL of propidium iodide (PI), the residues were incubated for another 15 min at room temperature in the dark. The stained cells were analyzed by a flow cytometer (BD Accuri C6).

4.13. Induction of autophagy

Autophagy induced by compound **15e** in A549 cells was detected using the Lyso-Tracker Green DND-26 and the DAPRed Autophagy detection kit. Briefly, approximately 5×10^4 A549 cells were seeded on a cell culture dish (diameter = 35 mm) and incubated for 24 h. The medium was replaced by fresh medium containing 100 nM DAPRed Dye. After incubation for 30 min, the cells were rinsed with PBS three times and incubated with fresh medium containing 0.1 μM **15e** for another 24 h in the dark. The Lyso-Tracker Green DND-26 probe (100 nM) was added at 1.0 h after the cells were exposed to a laser at 660 nm for a light dose of 1.0 J/cm^2 or kept in the dark. After incubation for another 1.5 h, the cells were then rinsed with PBS three times again and examined using a Leica TCS SP5 spectral confocal microscope equipped with Argon-HeliumNenon (Ar-HeNe) laser. Lyso-Tracker and DAPRed were excited at the wavelength of 488 nm and 561 nm, respectively.

Declaration of competing interest

The authors declare that they have no known competing financial interests or personal relationships that could have appeared to influence the work reported in this paper.

Acknowledgements

This work was supported by the Natural Science Foundation of China (Grant No. 81172950 and 81671739), the Project of Science and Technology Commission of Shanghai (Grant No. 11431920401).

Appendix A. Supplementary data

Supplementary data to this article can be found online at https://doi.org/10.1016/j.ejmech.2021.113363.

References

[1] A.P. Castano, P. Mroz, M.R. Hamblin, Photodynamic therapy and anti-tumour immunity, Nat. Rev. Canc. 6 (2006) 535–545.
[2] P. Agostinis, K. Berg, K.A. Cengel, T.H. Foster, A.W. Girotti, S.O. Gollnick, S.M. Hahn, M.R. Hamblin, A. Juzeniene, D. Kessel, Photodynamic therapy of cancer: an update, CA-Cancer J. Clin. 61 (2011) 250–281.
[3] M. Ethirajan, Y. Chen, P. Joshi, R.K. Pandey, The role of porphyrin chemistry in tumor imaging and photodynamic therapy, Chem. Soc. Rev. 40 (2011) 340–362.
[4] H. Abrahamse, M.R. Hamblin, Review article: new photosensitizers for photodynamic therapy, Biochem. J. 473 (2016) 347–364.
[5] J.P. Celli, B.Q. Spring, I. Rizvi, C.L. Evans, K.S. Samkoe, S. Verma, B.W. Pogue, T. Hasan, Imaging and photodynamic therapy: mechanisms, monitoring, and optimization, Chem. Rev. 110 (2010) 2795–2838.
[6] W. Fan, P. Huang, X. Chen, Overcoming the Achilles' heel of photodynamic therapy, Chem. Soc. Rev. 45 (2016) 6488–6519.
[7] A.M. Bugaj, Targeted photodynamic therapy–a promising strategy of tumor treatment, Photochem. Photobiol. Sci. 10 (2011) 1097–10109.
[8] W. Sharman, Targeted photodynamic therapy via receptor mediated delivery systems, Adv. Drug Deliv. Rev. 56 (2004) 53–76.
[9] L. Li, Z. Luo, Z. Chen, J. Chen, S. Zhou, P. Xu, P. Hu, J. Wang, N. Chen, J. Huang, M. Huang, Enhanced photodynamic efficacy of zinc phthalocyanine by conjugating to heptalysine, Bioconjugate Chem. 23 (2012) 2168–2172.
[10] A.F. Hussain, F. Kampmeier, V. von Felbert, H.F. Merk, M.K. Tur, S. Barth, SNAP-tag technology mediates site specific conjugation of antibody fragments with a photosensitizer and improves target specific phototoxicity in tumor cells, Bioconjugate Chem. 22 (2011) 2487–2495.
[11] C.S. Ferreira, M.C. Cheung, S. Missailidis, S. Bisland, J. Gariepy, Phototoxic aptamers selectively enter and kill epithelial cancer cells, Nucleic Acids Res. 37 (2009) 866–876.
[12] P. Mallikaratchy, Z. Tang, W. Tan, Cell specific aptamer-photosensitizer conjugates as a molecular tool in photodynamic therapy, ChemMedChem 3 (2008) 425–428.
[13] D. Li, P. Li, H. Lin, Z. Jiang, L. Guo, B. Li, A novel chlorin-PEG-folate conjugate with higher water solubility, lower cytotoxicity, better tumor targeting and photodynamic activity, J. Photochem. Photobiol., B 127 (2013) 28–37.
[14] R. Schneider, F. Schmitt, C. Frochot, Y. Fort, N. Lourette, F. Guillemin, J.F. Müller, M. Barberi-Heyob, Design, synthesis, and biological evaluation of folic acid targeted tetraphenylporphyrin as novel photosensitizers for selective photodynamic therapy, Bioorg. Med. Chem. 13 (2005) 2799–2808.
[15] I.R. Vlahov, C.P. Leamon, Engineering folate-drug conjugates to target cancer: from chemistry to clinic, Bioconjugate Chem. 23 (2012) 1357–1369.
[16] Z. Meng, B. Shan, L. Zhang, G. Han, M. Liu, N. Jia, Z. Miao, W. Zhang, C. Sheng, J. Yao, Amino acid derivatives of pyropheophorbide-a ethers as photosensitizer: synthesis and photodynamic activity, Chin. Chem. Lett. 27 (2016) 623–626.
[17] Z. Meng, B. Yu, G. Han, M. Liu, B. Shan, G. Dong, Z. Miao, N. Jia, Z. Tan, B. Li, W. Zhang, H. Zhu, C. Sheng, J. Yao, Chlorin p6-based water-soluble amino acid derivatives as potent photosensitizers for photodynamic therapy, J. Med. Chem. 59 (2016) 4999–5010.
[18] X. Zhang, Z. Meng, Z. Ma, J. Liu, G. Han, F. Ma, N. Jia, Z. Miao, W. Zhang, C. Sheng, J. Yao, Design and synthesis of novel water-soluble amino acid derivatives of chlorin p_6 ethers as photosensitizers, Chin. Chem. Lett. 30 (2019) 247–249.
[19] R.G. Jinadasa, X. Hu, M.G. Vicente, K.M. Smith, Syntheses and cellular investigations of 17^3-, 15^2-, and 13^1-amino acid derivatives of chlorin e_6, J. Med. Chem. 54 (2011) 7464–7476.
[20] A. Fadlan, H. Tanimoto, T. Ito, Y. Aritomi, M. Ueno, M. Tokuda, S. Hirohara, M. Obata, T. Morimoto, K. Kakiuchi, Synthesis, photophysical properties, and photodynamic activity of positional isomers of TFPP-glucose conjugates, Bioorg. Med. Chem. 26 (2018) 1848–1858.
[21] P.M.R. Pereira, W. Rizvi, N. Bhupathiraju, N. Berisha, R. Fernandes, J.P.C. Tome, C.M. Drain, Carbon-1 versus carbon-3 linkage of d-galactose to porphyrins: synthesis, uptake, and photodynamic efficiency, Bioconjugate Chem. 29 (2018) 306–315.
[22] Z. Ma, P. Hu, C. Guo, D. Wang, X. Zhang, M. Chen, Q. Wang, M. Sun, P. Zeng, F. Lu, L. Sun, L. She, H. Zhang, J. Yao, F. Yang, Folate-mediated and pH-responsive chidamide-bound micelles encapsulating photosensitizers for tumor-targeting photodynamic therapy, Int. J. Nanomed. 14 (2019) 5527–5540.
[23] F.L. Zhang, M.R. Song, G.K. Yuan, H.N. Ye, Y. Tian, M.D. Huang, J.P. Xue, Z.H. Zhang, J.Y. Liu, A molecular combination of zinc(II) phthalocyanine and tamoxifen derivative for dual targeting photodynamic therapy and hormone therapy, J. Med. Chem. 60 (2017) 6693–6703.
[24] S. Zakaria, A.M. Gamal-Eldeen, S.M. El-Daly, S. Saleh, Synergistic apoptotic effect of Doxil® and aminolevulinic acid-based photodynamic therapy on human breast adenocarcinoma cells, Photodiagn. Photodyn. 11 (2014) 227–238.
[25] V. Raju, N. Varukattu, R. Chandrababu, S. Alok, P. Thondhi, V. Alagarsamy, K. Soundarapandian, Multifunctional nanoparticles for trimodal photodynamic therapy-mediated photothermal and chemotherapeutic effects, Photodiagnosis Photodyn. Ther. 23 (2018) 244–253.
[26] Y. Han, Z. Chen, H. Zhao, Z. Zha, W. Ke, Y. Wang, Z. Ge, Oxygen-independent combined photothermal/photodynamic therapy delivered by tumor acidity-responsive polymeric micelles, J. Contr. Release 284 (2018) 15–25.
[27] C. Zhang, L. Gao, Y. Cai, H. Liu, D. Gao, J. Lai, B. Jia, F. Wang, Z. Liu, Inhibition of tumor growth and metastasis by photoimmunotherapy targeting tumor-associated macrophage in a sorafenib-resistant tumor model, Biomaterials 84 (2016) 1–12.
[28] P.A. Jones, J.P. Issa, S. Baylin, Targeting the cancer epigenome for therapy, Nat. Rev. Genet. 17 (2016) 630–641.
[29] B.E. Gryder, Q.H. Sodji, A.K. Oyelere, Targeted cancer therapy: giving histone deacetylase inhibitors all they need to succeed, Future Med. Chem. 4 (2012) 505–524.
[30] A.C. West, R.W. Johnstone, New and emerging HDAC inhibitors for cancer treatment, J. Clin. Invest. 124 (2014) 30–39.
[31] X. Li, Y.K. Peterson, E.S. Inks, R.A. Himes, J. Li, Y. Zhang, X. Kong, C.J. Chou, Class I HDAC inhibitors display different antitumor mechanism in leukemia and prostatic cancer cells depending on their p53 status, J. Med. Chem. 61 (2018) 2589–2603.
[32] B.S. Mann, J.R. Johnson, M.H. Cohen, R. Justice, R. Pazdur, FDA approval summary: vorinostat for treatment of advanced primary cutaneous T-cell lymphoma, Oncology 12 (2007) 1247–1252.
[33] H. Bailey, D.D. Stenehjem, S. Sharma, Panobinostat for the treatment of multiple myeloma: the evidence to date, J. Blood Med. 6 (2015) 269–276.
[34] K. Ververis, A. Hiong, T.C. Karagiannis, P.V. Licciardi, Histone deacetylase inhibitors (HDACIs): multitargeted anticancer agents, Biologics 7 (2013) 47–60.
[35] M. Manal, M.J. Chandrasekar, J. Gomathi Priya, M.J. Nanjan, Inhibitors of histone deacetylase as antitumor agents: a critical review, Bioorg. Chem. 67 (2016) 18–42.
[36] B.E. Gryder, Q.H. Sodji, A.K. Oyelere, Targeted cancer therapy: giving histone deacetylase inhibitors all they need to succeed, Future Med. Chem. 4 (2012) 505–524.
[37] Y. Huang, G. Dong, H. Li, N. Liu, W. Zhang, C. Sheng, Discovery of janus kinase 2 (JAK2) and histone deacetylase (HDAC) dual inhibitors as a novel strategy for combinational treatment of leukemia and invasive fungal infections, J. Med. Chem. 61 (2018) 6051–6074.
[38] J.J. McClure, X. Li, C.J. Chou, Advances and challenges of HDAC inhibitors in cancer therapeutics, Adv. Canc. Res. 138 (2018) 183–211.
[39] E.H. Rubin, N.G. Agrawal, E.J. Friedman, P. Scott, K.E. Mazina, L. Sun, L. Du, J.L. Ricker, S.R. Frankel, K.M. Gottesdiener, J.A. Wagner, M. Iwamoto, A study to determine the effects of food and multiple dosing on the pharmacokinetics of vorinostat given orally to patients with advanced cancer, Clin. Canc. Res. 12 (2006) 7039–7045.
[40] Q.C. Ryan, D. Headlee, M. Acharya, A. Sparreboom, J.B. Trepel, J. Ye, W.D. Figg, K. Hwang, E.J. Chung, A. Murgo, G. Melillo, Y. Elsayed, M. Monga, M. Kalnitskiy, J. Zwiebel, E.A. Sausville, Phase I and pharmacokinetic study of MS-275, a histone deacetylase inhibitor, in patients with advanced and refractory solid tumors or lymphoma, J. Clin. Oncol. 23 (2005) 3912–3922.
[41] G. Dong, W. Chen, X. Wang, X. Yang, T. Xu, P. Wang, W. Zhang, Y. Rao, C. Miao, C. Sheng, Small molecule inhibitors simultaneously targeting cancer metabolism and epigenetics: discovery of novel nicotinamide phosphoribosyltransferase (NAMPT) and histone deacetylase (HDAC) dual inhibitors, J. Med. Chem. 60 (2017) 7965–7983.
[42] K.B. Daniel, E.D. Sullivan, Y. Chen, J.C. Chan, P.A. Jennings, C.A. Fierke, S.M. Cohen, Dual-mode HDAC prodrug for covalent modification and subsequent inhibitor release, J. Med. Chem. 58 (2015) 4812–4821.
[43] P.T. Li, Y.J. Tsai, M.J. Lee, C.T. Chen, Increased histone deacetylase activity involved in the suppressed invasion of cancer cells survived from ALA-mediated photodynamic treatment, Int. J. Mol. Sci. 16 (2015) 23994–24010.
[44] R.R. Ye, C.P. Tan, L. He, M.H. Chen, L.N. Ji, Z.W. Mao, Cyclometalated Ir(III) complexes as targeted theranostic anticancer therapeutics: combining HDAC inhibition with photodynamic therapy, Chem. Commun. (Camb) 50 (2014) 10945–10948.
[45] J.J. Sung, K. Ververis, T.C. Karagiannis, Histone deacetylase inhibitors potentiate photochemotherapy in cutaneous T-cell lymphoma MyLa cells,

J. Photochem. Photobiol., B 131 (2014) 104–112.
[46] J. Yao, W. Zhang, C. Sheng, Z. Miao, F. Yang, J. Yu, L. Zhang, Y. Song, T. Zhou, Y. Zhou, Design, synthesis, and in vitro photodynamic activities of benzochloroporphyrin derivatives as tumor photosensitizers, Bioorg. Med. Chem. Lett 18 (2008) 293–297.
[47] J. Zhang, L. Deng, J. Yao, P. Gu, F. Yang, X. Wang, W. Liu, Y. Zhang, J. Ke, X. Jing, J. Chen, Synthesis and photobiological study of a novel chlorin photosensitizer BCPD-18MA for photodynamic therapy, Bioorg. Med. Chem. 19 (2011) 5520–5528.
[48] M. Sun, C. Zhou, H. Zeng, F. Yin, Z. Wang, J. Yao, Y. Hua, Z. Cai, Benzochloroporphyrin derivative photosensitizer-mediated photodynamic therapy for Ewing sarcoma, J. Photochem. Photobiol., B 160 (2016) 178–184.
[49] J. Yao, W. Zhang, L. Zhang, H. Zheng, Y. Zhou, A new preparation of chlorin f, Chin. J. Pharm. 34 (2003) 267–268.
[50] Z. Yu, Q. Sun, W. Pan, N. Li, B. Tang, A near-infrared triggered nano photosensitizer inducing domino effect on mitochondrial reactive oxygen species burst for cancer therapy, ACS Nano 9 (2015) 11064–11074.
[51] R.G.W. Jinadasa, H. Xiaoke, M.G.A.H. Vicente, K.M. Smith, Syntheses and cellular investigations of 17(3)-, 15(2)-, and 13(1)-amino acid derivatives of chlorin e(6), J. Med. Chem. 54 (2011) 7464–7476.
[52] S. Rangasamy, H. Ju, S. Um, D.-C. Oh, J.M. Song, Mitochondria and DNA targeting of 5, 10, 15, 20-tetrakis (7-sulfonatobenzo [b] thiophene) porphyrin-induced photodynamictherapy via intrinsic and extrinsic apoptotic cell death, J. Med. Chem. 58 (2015) 6864–6874.
[53] J.F. Chiou, Y.H. Wang, M.J. Jou, T.Z. Liu, C.Y. Shiau, Verteporfin-photoinduced apoptosis in HepG2 cells mediated by reactive oxygen and nitrogen species intermediates, Free Radic. Res. 44 (2010) 155–170.
[54] C. He, D.J. Klionsky, Regulation mechanisms and signaling pathways of autophagy, Annu. Rev. Genet. 43 (2009) 67–93.
[55] N. Mizushima, M. Komatsu, Autophagy: renovation of cells and tissues, Cell 147 (2011) 728–741.
[56] L. Yu, Y. Chen, S.A. Tooze, Autophagy pathway: cellular and molecular mechanisms, Autophagy 14 (2018) 207–215.